

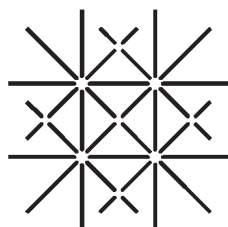
# 2D Bimolecular Self-Assembled Porphyrin-Fullerene Nanostructures

**Inauguraldissertation**

zur  
Erlangung der Würde eines Doktors der Philosophie  
vorgelegt der  
Philosophisch-Naturwissenschaftlichen Fakultät  
der Universität Basel  
von

Andreas Kiebele  
aus Aesch (BL)

Basel, 2006



**UNI  
BASEL**

Genehmigt von der Philosophisch-Naturwissenschaftlichen Fakultät auf Antrag  
von

Prof. Dr. H.-J.Güntherodt

Prof. Dr. E. Meyer

Dr. H. Spillmann

Basel, den 19.12.06

Prof. Dr. Hans-Peter Hauri, Dekan

# Abstract

The formation of self-assembled monolayers of porphyrin molecules and their usefulness as surface supported templates for hosting fullerene molecules has been investigated by means of a room temperature Scanning Tunneling Microscope (STM). In particular, examples of unprecedented addressable supramolecular architectures composed of fullerenes and porphyrins were obtained. Furthermore, the first 2-dimensional porphyrin based supramolecular host network with porous structure has been self-assembled on a solid surface. This network features a specific chemical sensitivity for different fullerene guest molecules.

Various porphyrin derivatives were deposited onto diverse metal substrates. While some combinations did not result in ordered monolayers, many others revealed to form self-assembled structures. Two varieties of porphyrin molecules were examined. On the one hand, single porphyrin cores featuring different functional side-groups were investigated. On the other hand, unique triply-fused diporphyrin cores, also featuring relevant functional groups, have been researched. In addition to several close-packed monolayers, a nanoporous assembly of porphyrin molecules was discovered. This porous network features cavities with a pore-size approximately identical to the size of  $C_{60}$  fullerenes and a pore-pore distance of 3.3 nm. Fullerene molecules were adsorbed onto preformed porphyrin assemblies. Several of these monolayers exhibit interesting fullerene hosting capabilities. The fullerenes have been found to form lines, pairs or adsorb into the pores depending on the underlying porphyrin structure. In particular, the adsorption and dynamics of  $C_{60}$  and  $C_{70}$  fullerenes hosted in the self-assembled nanoporous network on the Ag(111) surface have been studied. Time-resolved STM studies of these supramolecular systems have revealed host-guest interactions resulting in a distinctly dissimilar mobility of the two fullerenes within the porous porphyrin network. Long-range coverage-dependent interactions have been discovered to influence the hopping rates of the adsorbed fullerene guests. These are likely mediated by a complex mechanism involving both the Ag substrate and the flexible porphyrin host network. At increased fullerene coverage this unprecedented interplay results in the formation of large fullerene chains and islands. By applying a lattice gas model with nearest-neighbor interactions and by evaluating the fullerene pair distribution functions the respective coverage-dependent guest-guest interaction energies have been estimated.





# Contents

<b>Abstract</b>	<b>i</b>
<b>List of Figures</b>	<b>vi</b>
<b>Abbreviations</b>	<b>vii</b>
<b>1 Introduction</b>	<b>1</b>
1.1 Self-Assembly . . . . .	2
1.2 Molecules . . . . .	3
1.2.1 Porphyrin Derivatives . . . . .	3
1.2.2 Fullerenes . . . . .	4
1.2.3 Safety of Nanomaterials . . . . .	6
<b>2 Experimental Methods and Set-up</b>	<b>9</b>
2.1 Scanning Tunneling Microscope (STM) . . . . .	10
2.1.1 Basic Principles of the STM . . . . .	11
2.1.2 Advanced STM Theory . . . . .	12
2.1.3 Manipulating Single Molecules with the STM . . . . .	15
2.2 Sample Preparation . . . . .	16
2.2.1 Atomically Flat and Clean Substrates . . . . .	16
2.2.2 Molecule Deposition . . . . .	17
<b>3 Diporphyrin Assemblies</b>	<b>19</b>
3.1 DDP Assemblies on Ag(100) . . . . .	19
3.2 pDDP Assemblies on Ag(100) . . . . .	22
3.3 The Importance of the Functional Groups for the Self-Assembly . . . . .	25
3.4 C <sub>60</sub> - DDP Assemblies on Ag(100) . . . . .	26
3.5 Upside Down: Porphyrin deposition on C <sub>60</sub> Monolayers . . . . .	28
<b>4 Monoporphyrin Assemblies</b>	<b>31</b>
4.1 DMP Assemblies on Ag(100) . . . . .	32
4.2 DMP on Cu(111) . . . . .	32
4.3 DMP Assemblies on Ag(111) . . . . .	35
4.4 The Importance of the Substrate for the Self-Assembly . . . . .	39

4.5	C <sub>60</sub> - DMP Assemblies on Ag(100) . . . . .	42
4.6	C <sub>60</sub> - DMP Assemblies on Ag(111) . . . . .	42
<b>5</b>	<b>Adsorption and Dynamics of Hosted Fullerenes</b>	<b>47</b>
5.1	Adsorption of C <sub>60</sub> and C <sub>70</sub> in the Host-Network . . . . .	47
5.2	Mobility of Single Fullerene Molecules . . . . .	50
5.3	Jump Lengths . . . . .	52
5.4	Coverage Dependent Hopping Rates . . . . .	52
5.5	Pair Distribution . . . . .	57
5.6	Long-Range Interactions . . . . .	59
<b>6</b>	<b>Conclusion and Outlook</b>	<b>63</b>
	<b>Bibliography</b>	<b>65</b>
	<b>Acknowledgements</b>	<b>75</b>
	<b>Publications and Conferences</b>	<b>77</b>
	<b>Curriculum Vitae</b>	<b>79</b>

# List of Figures

1.1	Chemical structures of the porphyrins . . . . .	4
1.2	Fullerenes: $C_{60}$ and $C_{70}$ . . . . .	5
2.1	Multi-chamber UHV system . . . . .	9
2.2	Classical vs. QM potential barrier . . . . .	10
2.3	Schematic energy diagram for the one dimensional tunneling process	11
2.4	STM image showing effects of tip change . . . . .	14
3.1	Structures of DDP and pDDP . . . . .	20
3.2	STM image of DDP molecules on Ag(100) . . . . .	21
3.3	Model of DDP adsorbed on Ag(100) . . . . .	22
3.4	STM image showing ordered- and gas-phase of DDP on Ag(100) .	23
3.5	STM image of pDDP on Ag(100) . . . . .	24
3.6	Model of pDDP on Ag(100) . . . . .	25
3.7	STM image and model of $C_{60}$ - DDP assemblies on Ag(100) . . .	27
3.8	STM image of $C_{60}$ manipulation sequence . . . . .	28
3.9	STM images of DDP molecules deposited on preadsorbed $C_{60}$ ML	29
4.1	Structure of DMP . . . . .	31
4.2	STM image and model of DMP on Ag(100) . . . . .	33
4.3	STM images of DMP on Cu(111) . . . . .	34
4.4	Model of DMP adsorbed on Cu(111) . . . . .	35
4.5	STM image and model of close-packed assembly of DMP on Ag(111)	36
4.6	STM image of the porous assembly of DMP on Ag(111) . . . . .	37
4.7	Model of porous DMP assembly on Ag(111) . . . . .	38
4.8	STM images of $C_{60}$ on DMP on Ag(100) . . . . .	42
4.9	STM images of $C_{60}$ on the porous DMP assembly on Ag(111) . .	43
4.10	Model of a $C_{60}$ adsorbed on the porous DMP assembly on Ag(111)	44
4.11	STM images of $C_{60}$ -pair phase on DMP on Ag(111) . . . . .	45
5.1	Line sections of the porphyrin network . . . . .	48
5.2	Normalized histograms of the distribution of apparent heights . .	49
5.3	Series of consecutive STM images of fullerenes on porous DMP . .	50
5.4	Histogram of jump distances . . . . .	53

5.5	Coverage dependent hopping rate of $C_{60}$ and $C_{70}$ . . . . .	54
5.6	Interaction energies of the $C_{60}$ and $C_{70}$ . . . . .	56
5.7	Pair distribution $g(j)$ . . . . .	58
5.8	Time evolution of the conformations adopted by the 3,5-di(tert-butyl)phenyl substituents . . . . .	60

# Abbreviations

2D	Two-Dimensional
Ag	Silver
Au	Gold
CO	Carbon Monoxide
Cu	Copper
DOS	Density Of States
H-bond	Hydrogen-Bond
HOMO	Highest Occupied Molecular Orbital
LDOS	Local Density Of States
LEED	Low Energy Electron Diffraction
LUMO	Lowest Unoccupied Molecular Orbital
ML	Monolayer
MO	Molecular Orbital
Ni	Nickel
RT	Room Temperature
STM	Scanning Tunneling Microscope
UHV	Ultra High Vacuum
UPS	UV Photoelectron Spectroscopy
vdW	van der Waals
Xe	Xenon
XPS	X-ray Photoelectron Spectroscopy
Zn	Zinc



# Chapter 1

## Introduction

There are two main reasons for the ongoing interest in nanoscale science. Firstly, the materials examined in this field promise a new manufacturing technique known as *bottom-up* which allows for the construction of extended architectures featuring extremely small functionalities. Current technology depends on miniaturization of well understood systems. The most common and successful example of this process is the incredible progress in the fabrication of silicon-based microchips. The production of these chips employs the so-called *top-down* approach which means that the chips are being produced from one piece by removing the unwanted parts (e.g. through lithography) leaving only the structures required for the device to work. However, there are fundamental physical limits as well as economical limits posing problems for this approach [1]. Large investments in R&D and production equipment have been made in order to keep up with the progress (while decreasing the 'cost per function') [2]. The opposite approach, namely taking the smallest possible functional units such as single atoms or molecules and assembling those into devices is called *bottom-up* approach. Notably, this approach is also employed by nature to form proteins and even whole cells [3] obviously with very successful results.

The other reason is the fact that well known materials such as carbon or metals exhibit remarkable effects when one or more dimensions are below a certain critical size. Usually, structures are referred to as being *nanost*tructures when the important dimension(s) are below 100 nm. Interesting novel catalytic, magnetic, mechanical and optical properties have been found [4]. Networks consisting of metal organic molecules as examined in this work with pores and pore-pore distances of nanoscale size are particularly interesting. Their chemical versatility and structural similarity to zeolites makes them promising candidates for the fabrication of multifunctional materials with various potential applications as catalysts, molecular sieves, shape- and size-selective recognition and chemical sensors [5–9].

In this thesis the properties of porphyrin molecules adsorbed on metal surfaces will be examined. The influence of different functional groups and different substrates on the ordering behavior will be discussed in chapters 3 and 4. While this is only the subordinate target it is important to gain some insight into these correlations in order to achieve the second goal. The superordinate target is to investigate the possibility of using these porphyrin monolayers as templates for structuring surfaces for the purpose of hosting fullerene guest molecules in a controlled manner. Various cases of organized porphyrin structures hosting C<sub>60</sub> throughout chapters 3 and 4 exhibiting various interesting properties will be shown. Furthermore, chapter 5 provides deeper insights into the interesting host-host and host-guest interactions present in one of these systems composed of porphyrins hosting C<sub>60</sub> and C<sub>70</sub> molecules.

## 1.1 Self-Assembly

The terms "self-assembly" and "self-organization" have been defined with slightly different meanings in various publications [3,10–12], sometimes with interchangeable meanings. For the scope of this work the best fitting definition is probably the one given by Whitesides et al.: "Molecular self-assembly is the spontaneous association of molecules under equilibrium conditions into stable, structurally well-defined aggregates joined by noncovalent bonds" [12]. It is worth noting that this definition is roughly equivalent to the one given by Lehn for *supramolecular* self-assembly [10], while he considers molecular self-assembly as a chemical process involving covalent bonds. The key points of the definition of self-assembly are as follows. First, the molecules involved assemble into structures held together by non-covalent bonds. The molecules are thus held together either by electrostatic forces (e.g. dipole-dipole-interactions), electro-dynamic forces (e.g. van der Waals (vdW) interaction) or hydrogen or coordination bonds. Secondly, the ordered phase must be in a thermodynamic equilibrium. For example, a structure which only exists while increasing the temperature or number of molecules and disappears afterwards would not be considered self-assembly in this sense. Although the formation of a specific self-assembled structure may need energy (e.g. thermal annealing of the sample) the resulting structure, once formed, is stable [3].

In order for molecules to be able to self-assemble the adsorbed molecules need to be mobile. Otherwise the molecules would stick where they were adsorbed and form a random pattern according to their statistical distribution. However, the resulting structure must be energetically favorable (energetic minimum). Since all the structures shown in this work are measured at room temperature (RT) one can estimate the binding energy of the structure to be greater than  $kT$  ( $k$ : Boltzmann's constant,  $T$ : temperature) which is approximately 26 meV at RT.



## 1.2 Molecules

The molecules presented in this work can be divided into two categories: the all carbon fullerenes (chapter 1.2.2) and the metal-organic porphyrins (chapter 1.2.1) which will be discussed in detail in the respective chapters. Some properties are common to all the substances used, due to the requirement of the experimental setup. They must be very pristine, they must be solid at RT, and one must be able to evaporate them without breaking intramolecular bonds (for details see 2.2.2).

### 1.2.1 Porphyrin Derivatives

One family of compounds used in this work are the so called porphyrins. Their name is derived from the Greek word for purple: *porphura*. All porphyrins are chromophores (absorb visible light) [13] and thus appear colored to the human eye. Porphyrin derivatives have first been synthesized in 1929 [13] and in 1959 the first crystal structure of a porphyrin derivative has been reported [14]. The chemical structure of the tetrapyrrolic macrocycles can be seen in figure 1.1. Four pyrrole rings are linked by four methyne bridges and build an extended aromatic  $\pi$ -system which includes 18  $\pi$ -electrons per porphyrin core [15]. The molecule features a rigid planar structure with a fourfold symmetry. Together with a metallic center (in this work always Zn) the porphyrin can form a metallocomplex. It has been shown in solution that porphyrins may act as electron donors for  $C_{60}$  [15]. The porphyrin macrocycles can be augmented with functional groups at many different positions. In this study some of those groups are 3,5-di(*tert*-butyl)phenyl moieties which mainly act as spacers to avoid direct contact between the porphyrin core and metal substrate. The positions denominated by R can feature different functional groups. The composition and their relevance will be discussed in the appropriate chapters.

In nature porphyrin derivatives play a major role. Two very important examples are photosynthesis and oxygen transport. The photosynthesis in plants and algae use chlorophylls which are magnesium(II)-chlorin complexes with chlorin being a porphyrin derivative. To allow for photosynthesis the porphyrins absorb red light and thus are responsible for the green color of plants. In the metabolism of mammals, hemoglobin is responsible for oxygen transport. A part of this protein is the heme group, an iron(III)-porphyrin derivative [15].

In addition to the mono-porphyrins discussed above we were also able to study triply fused di-porphyrin derivatives shown in figure 1.1b. The two porphyrin macrocycles are arranged coplanar due to the rigid bonding between three carbon atoms of each porphyrin. This arrangement features the added value of extending the conjugated  $\pi$ -system to include both macrocycles at once. Again,

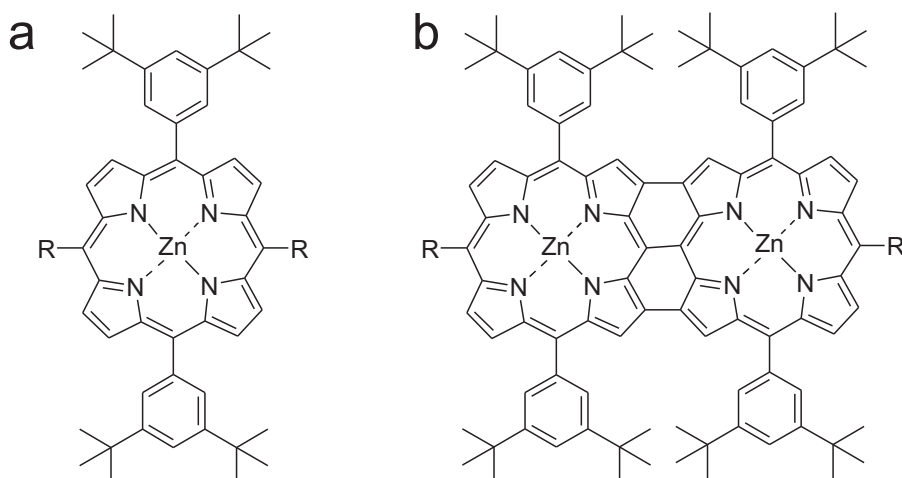


Figure 1.1: Chemical structures of the porphyrins.

the positions marked with R have been substituted with functional groups in order to allow self-assembly on surfaces.

### 1.2.2 Fullerenes

In 1985 H.W. Kroto et al. discovered large molecules consisting of carbon atoms. The name they proposed for the  $C_{60}$  molecule in their original paper [16] was Buckminsterfullerene in tribute to R. Buckminster Fuller who is best known for his work concerning the geodesic dome. Many closed cage all-carbon molecules of different size have since been discovered ranging from  $C_n$  with  $n=36$  to bigger ones with  $n=60$ , 70 and 78 up to  $n=90$  and 96 to name only a few. This class of compounds has since become known as fullerenes. More than 20 stable fullerenes between  $n=60$  and  $n=96$  have already been characterized [17]. In 1996 Robert F. Curl, Harold W. Kroto and Richard E. Smalley have been awarded the nobel prize in chemistry "for their discovery of fullerenes" [18]. Since 1990,  $C_{60}$  can be produced and isolated in macroscopic quantities [19]. Nowadays,  $C_{60}$  and  $C_{70}$  along with many other fullerenes are commercially available in the required purity. In this work the fullerenes  $C_{60}$  and  $C_{70}$  were used. In figure 1.2 the structures of the two fullerenes are drawn to scale in order to reflect their respective sizes.

Fullerenes show interesting properties in the solid phase. For example, it has been shown that bulk  $C_{60}$  doped with alkali metals form a superconductive phase with a transition temperature of 33 K [20]. Furthermore, they are a well-loved adsorbate for surface science experiments, due to their properties (e.g. charge

transfer) and ease of use. Examples of research interest include adsorption of  $C_{60}$  on surfaces and thin film growth.

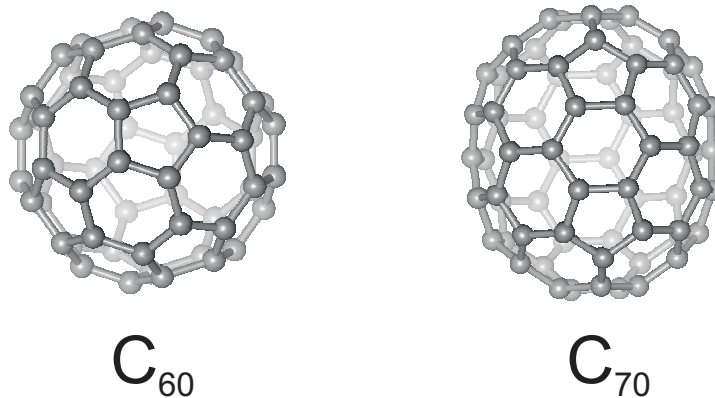


Figure 1.2: Molecular structure of the fullerenes used in this study. a)  $C_{60}$  Buckminsterfullerene, b)  $C_{70}$ .

### $C_{60}$ Buckminsterfullerene

$C_{60}$  is the most abundant member of the fullerene family. The structure of  $C_{60}$  resembles a round soccer ball made of hexagons and pentagons, with a carbon atom at the corners of each hexagon and a bond along each edge (figure 1.2a). None of the pentagonal rings make contact with each other. The diameter of the  $C_{60}$  cage is  $\approx 7 \text{ \AA}$  (center C atom to center C atom) and has a vdW diameter of  $d(C_{60}) \approx 10.6 \text{ \AA}$  [19, 21, 22]. The desorption temperature of bulk  $C_{60}$  is approximately 600 K.  $C_{60}$  has a large ionization potential of about 7.8 eV [17] compared to most surface work functions (e.g.  $\Phi_{Cu} = 4.6 \text{ eV}$ ,  $\Phi_{Au} = 5.4 \text{ eV}$  [23]) and a large electron affinity of  $\approx 2.7 \text{ eV}$ . Thus, it is not surprising that  $C_{60}$  acts as an electron acceptor. It adsorbs onto most metals (including Ag, Au and Cu) via charge transfer of up to 3 electrons per molecule (Ag(100) [17]), hence forming ionic bonds. Particularly for the substrates used in this study, namely Ag(100), Ag(111), and Cu(111) the electron transfer per  $C_{60}$  molecule is  $2.7 e^-$ ,  $0.75 e^-$  and  $1.6 e^-$  [24, 25].

$C_{60}$  adsorbed on noble metals preferably condense along step edges at low coverage. Increased coverage usually leads to hexagonal or quasi hexagonal arrangements of the molecules. For example on Ag(111)  $C_{60}$  arrange into a  $(2\sqrt{3} \times 2\sqrt{3})R \pm 30^\circ$  superstructure with respect to the metal lattice [26, 27]. On Ag(111) as well as on Ag(100) and Cu(111) contrast variations between the different adsorbed  $C_{60}$  can be seen. In the case of Ag(111) it seems to be due

to molecules bound in different rotational orientations [26]. However, the nature of this contrast difference of  $\approx 2 \text{ \AA}$  is still under debate. Either local surface reconstruction [28, 29] or electronic effects connected to the bonding of the  $C_{60}$  molecules with the substrate [30] are discussed.

## $C_{70}$

$C_{70}$  molecules are built analogical to  $C_{60}$  from hexagons and pentagons as shown in figure 1.2b. This structure can be formed by adding ten hexagons on the equator of the  $C_{60}$  cage. Due to the additional carbon atoms  $C_{70}$  has an ellipsoid shape with diameters of about  $7.0 \text{ \AA}$  and  $7.9 \text{ \AA}$  along the two axes of the cage (atom center to atom center). The vdW diameters of  $C_{70}$  are  $d_{min}(C_{70}) \approx 9.0 \text{ \AA}$  along the short axis and a maximal diameter of  $d_{max}(C_{70}) \approx 12.0 \text{ \AA}$  along the long axis<sup>1</sup>. The ionization potential of about  $7.3 \text{ eV}$  and electron affinity of about  $2.7 \text{ eV}$  for  $C_{70}$  are similar to the values found for  $C_{70}$ . Bulk  $C_{70}$  can be evaporated at a temperature of  $\approx 580 \text{ K}$  [31].

$C_{70}$  molecules deposited on metal substrates also form ordered layers with step edges providing the nucleation centers. On Cu(111) for example they assemble into a hexagonal structure just as  $C_{60}$  molecules do. By adopting an upright position (with the long axis perpendicular to the surface)  $C_{70}$  requires a similar lateral intermolecular distance. Thus  $C_{70}$  orders into the same  $4 \times 4$  reconstruction in respect to the surface [20, 32].

### 1.2.3 Safety of Nanomaterials

$C_{60}$  consists purely of carbon atoms just like graphite or diamond, for instance. Nevertheless,  $C_{60}$  molecules display distinctly different properties than bulk carbon substances. This is generally the case for nanomaterials like gold nanoclusters or fullerenes and the like. Of course this is exactly the reason why nanophysics is so interesting. New properties of relatively simple materials at the nanoscale can offer new possibilities for future technologies. However, those same properties may well prove harmful for the environment or people working with them. Nanoparticles occur naturally (e.g. in volcanoes and fires). Thus, the European Unions 'Scientific Committee on Emerging and Newly Identified Health Risks' (SCENIHR) concludes that "it would appear that there is no intrinsic risk associated with the nanoscale per se for the population as a whole" [33]. The

---

<sup>1</sup>vdW-volume and outer vdW-surface of  $C_{70}$  were evaluated by means of the volume and surface functions as implemented in the MOE (Molecular Operating Environment) package (Chemical Computing Inc., Montreal, 2004) version 2004.03, starting from the  $C_{70}$  crystal structure coordinates [21, 22]. The calculations have been performed on an Intel Xeon 3.0 GHz bi-processor workstation by D. Bonifazi et al. The corresponding vdW-diameters were estimated by approximating  $C_{70}$  as a prolate spheroid. For the short and long axis of the fullerene, values of  $d_{min} = 9.0 \pm 0.2$  and  $d_{max} = 12.0 \pm 0.2 \text{ \AA}$  were obtained.

SCENIHR Opinion then continues to list increased exposure levels (e.g. through large scale manufacturing of nanomaterials) for individuals and the environment as a whole to be a possible concern.

The biggest fear of nanotechnology in the general public is probably the scenario of the *grey goo* as described for example in the popular science-fiction book *Prey* by Michael Crichton [34]. In this scenario self-replicating nano-robots get out of control and destroy everything in their path. However, it is not clear if nanotechnology would ever be able to design such complex mechanisms on the required scale. Certainly today's technology is not this advanced and will not be for a while. It has even been pointed out that self-replication is not necessary or even efficient for possible future nano-manufacturing processes in a paper coauthored by the originator of the term *grey goo*, Eric Drexler [35]. The authors expect nano-manufacturing to have more general risks as they predict for the technology to have "the potential to profoundly disrupt economies and international relations" [35].

More immediate and concrete dangers are posed to people having direct contact with nanoparticles in science or industrial production, however. Production of macroscopic amounts of fullerenes is possible today while their properties are still under investigation. When applied to skin  $C_{60}$  exhibits only low toxicity. However, recent molecular dynamic simulations have shown that  $C_{60}$  can strongly bind to DNA molecules in aqueous solution. This could potentially deform and even damage the DNA [36]. Experimental results obtained *in vivo* using largemouth bass suggest that  $C_{60}$  can induce oxidative stress. In the brains of the exposed fish a significantly increase in oxidative damage could be measured as compared to the control group [37]. Fullerenes are almost insoluble in water but also chemically very inert [17]. Thus their impact on the environment and humans should be (and currently is) thoroughly investigated before large amounts are released into the environment to prevent damage as induced for example by the premature use of DDT [37] and to prevent policy makers to impose strict rules as happened with gene technology [38].

In our laboratory, only very small amounts of fullerenes are required and exposure is only possible while loading the evaporators with fresh molecules. The risks are thus very limited. Nevertheless, one should wear gloves while handling nanoparticles and avoid dispersing them in the air (e.g. when loading the evaporator, see section 2.2.2).



# Chapter 2

## Experimental Methods and Set-up

The experiments presented in this work were conducted in a multi-chamber ultra high vacuum (UHV) system located in the *Nanolab* (see figure 2.1). The measurements were done with a home built room temperature (RT) scanning tunneling microscope (STM). In chapter 2.1 an introduction to STM is given. In order to keep the samples clean of contamination all steps - cleaning, preparing and measuring of the sample - are conducted *in situ* under UHV conditions. The base pressure in our system is at about  $1 \times 10^{-10}$  mbar. To avoid cross contamination (e.g. molecule deposition contaminates STM chamber) the individual chambers are separated by valves. Sample cleaning and subsequent deposition of molecules are described in sections 2.2.1 and 2.2.2 respectively. More information concerning the *Nanolab* system can be found in [39–41].

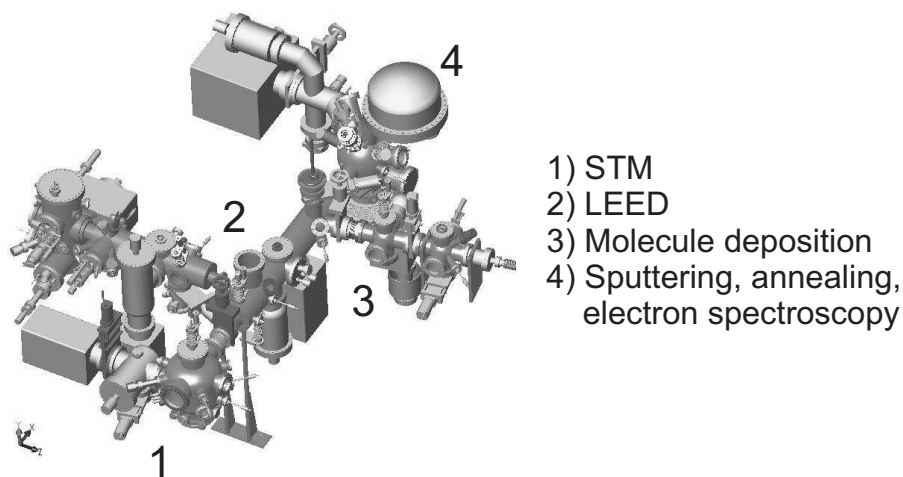


Figure 2.1: Multi-chamber UHV system in the *Nanolab*. The system features a RT STM, LEED, UPS, XPS and various cleaning and preparation possibilities. The chambers allow for *in situ* preparation and measurement under UHV conditions (base pressure  $\approx 10^{-10}$  mbar).

## 2.1 Scanning Tunneling Microscope (STM)

While working at IBM Research Laboratory in Rüschlikon, Gerd Binnig and Heinrich Rohrer developed the first STM [42]. An STM is able to image single molecules and even single atoms on electrically conductive surfaces. In 1986 Binnig and Rohrer were awarded the Nobel Prize in Physics "for their design of the scanning tunneling microscope" together with Ernst Ruska who was honored "for his fundamental work in electron optics, and for the design of the first electron microscope" [43]. Since the first example of obtaining atomic resolution on the reconstructed Si(111)- $7 \times 7$  surface [44] the STM was used to image countless metal and semiconductor surfaces, single molecules and molecule assemblies and even to manipulate single atoms and molecules in a controlled manner.

The STM consists of a very sharp metal tip which is brought into close proximity ( $\approx 5\text{-}15 \text{ \AA}$ ) of the sample which one desires to analyze without actually touching the two conductive pieces. It then utilizes the quantum mechanical effect of electron tunneling. This effect allows electrons, which would classically be restricted to the two conductors, to have a (small) finite possibility to penetrate the barrier. By applying a bias voltage between tip and sample a small current starts to flow. Using a piezo-electric actuator the tip is then scanned over the sample (x and y coordinates). There are two modes of measurement available: constant current and constant height. In constant height mode, the tip is moved over the sample at a constant height and the change in tunneling current is recorded. This mode is rarely used because of the high probability of the tip crashing into the sample. Constant current mode consists of a P-I controller trying to keep the current at the setpoint by controlling the z-movement (perpendicular to the sample) of the tip. The required movement is then recorded and displayed as a gray-scale or color-scale picture.

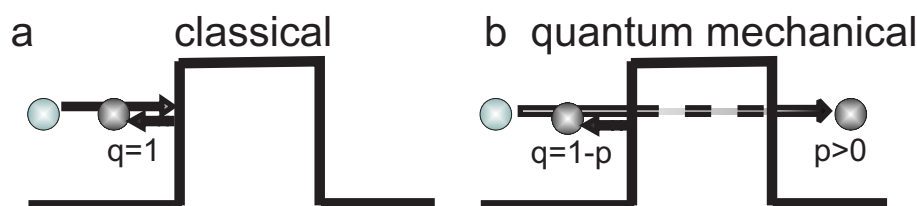


Figure 2.2: Schematic diagram of the classical and quantum mechanical potential barrier. While the electron cannot penetrate the barrier (reflection probability  $q = 1$ ) in the classical view (a), the electron has a certain probability  $p > 0$  in quantum mechanics (b) even though its energy is not sufficient to overcome the barrier.

Tunneling is a genuine quantum mechanical effect. In addition there are countless possible configurations possible for the tip and the sample. Thus the



problem can not be solved without applying simplifications. In the following sections the theoretical basis for imaging surfaces with the STM will be discussed in more detail. An overview can also be found in several textbooks [23, 45].

### 2.1.1 Basic Principles of the STM

In quantum mechanics the state of an electron is described by a wavefunction which satisfies the Schrödinger equation. The solution to this problem with a piecewise constant barrier yields for the classically not allowed region

$$\Psi(z) = \Psi(0)e^{-\kappa z} \quad (2.1)$$

with

$$\kappa = \frac{\sqrt{2m(V - E)}}{\hbar} \quad (2.2)$$

where  $E$  is the energy of the electron and  $V$  the potential barrier [23].

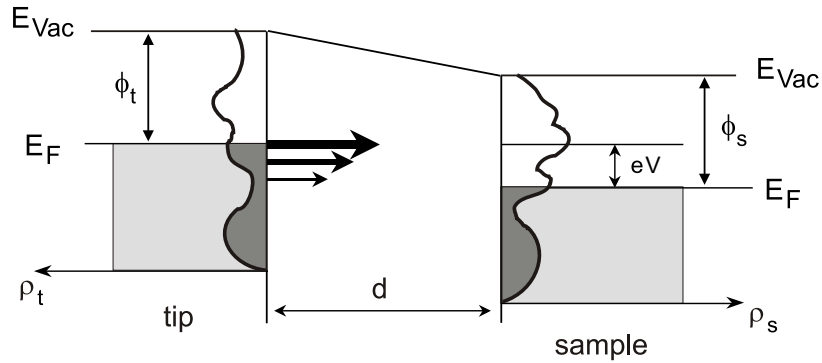


Figure 2.3: Schematic energy diagram for the one dimensional tunneling process between tip and sample.  $\rho_{s,t}$  indicate the respective density of states for the sample and the tip which are separated by a distance  $d$ . The arrows in the gap illustrate the probability for tunneling (greatest near Fermi energy  $E_F$ ) when a bias voltage  $V$  is applied.

By assuming a one-dimensional metal-vacuum-metal junction as depicted in figure 2.3 and applying a small bias voltage  $V$  one arrives at

$$I \propto V \rho_s(0, E_F) e^{-2\kappa d} \quad (2.3)$$

with

$$\kappa = \frac{\sqrt{2m\Phi}}{\hbar} \quad (2.4)$$

where  $\Phi$  denominates the work function. One can already see some important features of the STM, namely that there is a nonzero probability of the electron tunneling through the barrier which decays exponentially with the barrier thickness. In this model it is also assumed that the density of states at the Fermi level  $E_F$  does not vary significantly. Thus the current is proportional to the local density of states (LDOS) at  $E_F$ .

A more sophisticated model was developed by Tersoff and Hamann [46] based on the tunneling theory developed by Bardeen [47]. Assuming a tip shape in the form of a s-wavefunction and using several simplifications discussed below, they deduced the tunneling current to be

$$I \propto V \rho_t(E_F) \rho_s(z=0, E_F) e^{-2\kappa d} \quad (2.5)$$

with

$$\kappa = \frac{\sqrt{m(\Phi_s + \Phi_t)}}{\hbar} \quad (2.6)$$

where  $\rho_s$  and  $\rho_t$  denominate the density of states for the sample and the tip respectively and  $\Phi_s$  and  $\Phi_t$  are the respective work functions. If the tip does not change during an STM measurement, the Tersoff-Hamann theory predicts a behavior similar to equation 2.3. This model works well as a first approximation, especially when considering pure metal surfaces. However, the formula is only accurate if the following conditions apply [48, 49]:

- small bias voltages  $V \ll \Phi_{s,t}$  across the tunneling junction.
- low temperature, in order to approximate the Fermi-Dirac distribution as a step function.
- tip-sample distance of at least  $5 \text{ \AA}$ , so that the electronic states of the sample are not influenced by the tip.

Furthermore, electron-electron interactions are ignored in this model and the model can not explain lateral atomic resolution ( $\approx 2 \text{ \AA}$ )<sup>1</sup>.

### 2.1.2 Advanced STM Theory

Theoretically explaining the mechanisms an STM obeys to image atoms or molecules adsorbed on top of a surface is quite a challenge. The shape and amplitude of an adsorbate cannot easily be related to its structure. A well known example of counter intuitive behavior is CO adsorbed on metal surfaces which can appear as a protrusion of different shape and amplitude or even as a depression [51, 52].

<sup>1</sup>Chen solved this problem by applying p- and d-orbitals and the reciprocity principle to the above described perturbation theory [23, 50].

Modelling of such systems can generally be achieved by using a scattering theory formalism with specific models of the tip, barrier, and sample [48,51]. Basically this means that for every experiment a dedicated theoretical simulation has to be run. However there seem to be some features which are generally valid for imaging adsorbed molecules.

### **Imaging Single Molecules**

Let's consider a single molecule adsorbed on a surface. For one, the STM current is sensitive to the molecule-substrate interaction. Thus the STM image will be depending heavily on the binding sites of the molecules and the resulting symmetry. Also, calculations of the highest occupied molecular orbitals (HOMOs) and lowest unoccupied molecular orbitals (LUMOs) can give some indication of the image caused by an isolated molecule. However, for a correct simulation, inclusion of other molecular orbitals (MOs) and the substrate is required. In evaluating the contribution of a given MO to the tunneling current one has to consider two factors. First, the contribution of the MO is bigger the closer its energy is to the Fermi level. Secondly, the strength of the couplings of the MO with the surface and with the tip determine the strength of the tunneling current [51].

### **Imaging Dense Layers of Molecules**

This case introduces yet another possible complication. Even though the image of a layer of molecules may in some cases just be a simple superposition of isolated adsorbate images there is a possibility that some complex processes between the molecules will take place. For example, increasing the concentration of C adsorbed on Ni(111) leads to a decrease in the DOS on the surface around the Fermi level, causing the tip to move closer to the sample [53]. Furthermore, the tip geometry (see following section) may be of great importance, since the tip can couple simultaneously to different adatoms [51].

### **Tip Dependence**

Obviously, the shape and chemical structure of the tip can also influence the image recorded in an STM experiment. Sudden changes in the appearance, amplitude and shape of the imaged corrugations are commonly recorded during experiments, especially when measuring at RT and when working with high molecule coverage. These changes occur spontaneously by modifying the tip apex either by transferring a molecule between sample and tip or by atomic/molecular diffusion on the tip apex. Interestingly some of these tip dependent imaging changes are only visible when imaging layers of molecules and disappear when imaging single adsorbed molecules [51].

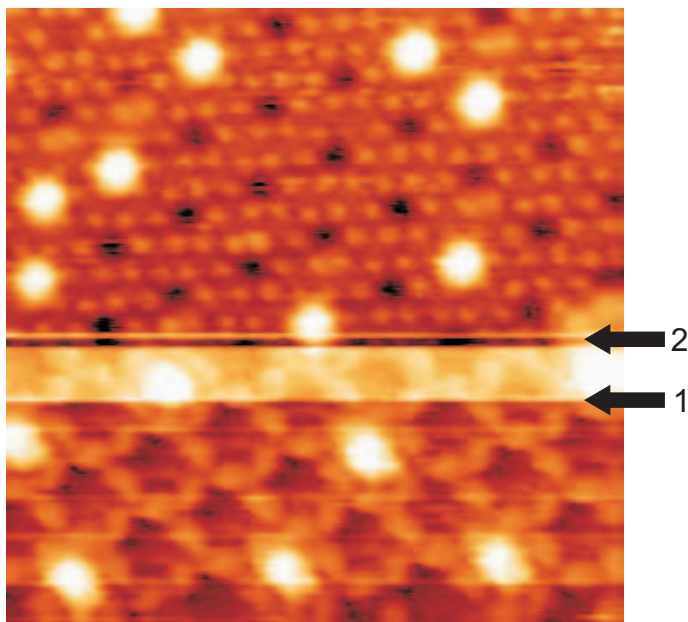


Figure 2.4: STM image (scan range:  $25 \times 25 \text{ nm}^2$ ,  $V_{bias} = 1.93 \text{ V}$ ,  $I_t = 9 \text{ pA}$ ,  $T = 298 \text{ K}$ ) showing effects of tip change. The arrows indicate the scan lines where the spontaneous tip changes have occurred.

An example of multiple tip changes in one STM image is given in figure 2.4 which was recorded from bottom to top. At the scan line marked with arrow 1 the tip changes such that the features are recorded in the same shape but with different apparent height. Arrow 2 indicates another modification in the tip structure which enables the STM to record more details than with the previous tip. Tip change 1 increases the apparent height of the molecule layer and the adsorbed guests. However, after the second change the details of the molecular layer are increased while the guest molecules (i.e. the molecules hosted in the porous network, see section 4.6 and chapter 5) seem to be imaged just as they were before the first change.

### Bias Voltage and Tip-Surface Dependence

Changing the applied bias voltage modifies the energy distribution of the electrons and thus probes different parts of the molecules electronic structure. Scanning tunneling spectroscopy (STS) has been developed to take advantage of this feature. Additionally, if the distance between tip and surface is decreased strong tip-surface interactions may start to affect the contrast of the STM images [51].

### 2.1.3 Manipulating Single Molecules with the STM

In order to laterally reposition molecules at room temperature the different forces which are acting on the adsorbate have to be balanced. On one hand the molecule must bind to the surface strong enough to prevent uncontrolled diffusion for a given corrugation of the surface potential and the thermal energy  $kT$ . At the same time the bonding has to be weak enough to allow for the STM tip to be able to induce controlled displacements of the adsorbate [54]. The search for suitable systems is particularly challenging because of the tendency of an adsorbate to stick firmly to the tip asperity instead of inducing the desired lateral manipulation. Thus appropriate parameters to avoid vertical movement or parameters to pick and place the molecules selectively back onto the substrate have to be found.

The first attempts to position atoms (e.g. xenon atoms on a nickel surface [55]) and molecules (e.g. CO on platinum [56] or copper [57–59]) were performed at low temperature to prevent unintentional effects due to the excitation by the thermal energy  $kT$ . Later, the first successful molecular manipulation experiments at room temperature were performed with porphyrin molecules on copper [54, 60]. Furthermore, molecular positioning experiments with  $C_{60}$  have been reported on many different substrates such as on Si(111)-(7 × 7) [61, 62], on Cu(100) [63] and on Cu(111) [64].

It is also important to note that at the single-molecule level the law of inertia does not have the same effect on the movement as in the macroscopic world. This is because it is the diffusion barrier height rather than the adsorbate mass which controls the relation between the net force applied to the adsorbate and its resulting acceleration [63]. Because of the very slow scanning speed of the STM tip the adsorbate is not provided with significant kinetic energy compared to the potential energy of the adsorbate in the surface potential corrugation.

There are basically three different modes to move a molecule. They are referred to as sliding, pulling and pushing [60, 63]. For large adsorbates like  $C_{60}$  at room temperature the pushing mode works best. This is because of the significant interaction of the large adsorbate with the substrate which is necessary in order to avoid temperature activated random diffusion. Here the repulsive Lennard-Jones potential with its high interaction force in the repulsive part offers the strong force to required induce lateral displacement. For pushing mode the tip is thus placed behind the adsorbate and then moved in the direction of the desired final position, as implied by the name. Another approach to manipulate molecules is to pick individual molecules up with the tip and place them again at a desired position [57].

Obviously, the molecule will not be displaced if this procedure is applied with the same parameters as used for non-distortive STM image acquisition. Previous experiments have shown that displacement of the adsorbate is preferentially induced at low gap resistance [54]. In other words the tunneling gap resistance is decreased by lowering the sample bias voltage and by increasing the tunneling current. This causes the tip height to be decreased in respect to the surface [61, 62]. The movement seems not to be induced with every trial. Thus, in most experiments mentioned above, the tip was swept several times over the surface. The same experiments indicate that some STM tips exhibit a much higher success rate for moving molecules than others, even if the same preparation is applied [61, 62, 65]. Reported success rates vary between 1:2 and 1:10 depending on the tip. Generally, tips with better image quality tend to be less suitable for positioning molecules [62].

## 2.2 Sample Preparation

### 2.2.1 Atomically Flat and Clean Substrates

In order to grow extended molecular assemblies one needs to start out with atomically clean substrates. Furthermore, they also need to feature well defined, flat terraces of appropriate size ( $> 50 \times 50 \text{ nm}^2$ ). The substrates used in this study are single crystals cut along distinct crystallographic directions as shown in table 2.1 with an accuracy better than  $0.4^\circ$  [40].

Substrate	Sputtering		Annealing	
	Acceleration [eV]	Time [min]	Current [A]	Time [min]
Ag(100)	700	17	3.1	60
Ag(111)	800	17	3.1	60
Cu(111)	800	17	3.8	60

Table 2.1: Substrates and corresponding cleaning parameters.

The substrates were cleaned by repeated cycles of  $\text{Ar}^+$  ion bombardment (sputtering) and thermal annealing. Parameters used for the sputtering process are listed in table 2.1. Usually, two or three sputtering-annealing cycles are sufficient to clean a substrate from the previously applied monolayer (ML) of molecules. The quality of this treatment has been regularly checked by STM. Furthermore, low energy electron diffraction (LEED) and X-ray photoemission spectroscopy (XPS) have initially been used to verify the crystallographic orientation and the absence of contaminations respectively.

## 2.2.2 Molecule Deposition

The organic molecules were deposited by sublimation from a resistively heated tantalum crucible (Knudsen-cell-type evaporator). The evaporators do not allow a direct temperature measurement. Instead the deposition temperature is set by applying a current (power supply running in current control mode) appropriate for the respective molecule (see table 2.2). During evaporation, the substrate was kept at room temperature (298 K). The deposition rate was controlled by a quartz microbalance. Previous experiments have shown that the thickness of the molecular layer can be reproducibly controlled within an error of 10% with this setup. Deposition rates were of the order of 0.5 to 2.0 Åmin<sup>-1</sup>.

Molecule	Rate [Åmin <sup>-1</sup> ]	$p_{max}$ [mbar]	Current [A]
C <sub>60</sub>	0.6 - 1.3	$3 \times 10^{-9}$	1.5 - 1.6
C <sub>70</sub>	0.5	$2 \times 10^{-9}$	1.6
DMP	1.5 - 2.0	$5 \times 10^{-9}$	1.5
DDP	0.9 - 2.0	$5 \times 10^{-7}$	1.8 - 2.0
pDDP	0.5 - 1.5	$1 \times 10^{-6}$	1.7 - 1.8

Table 2.2: Molecule deposition parameters.





# Chapter 3

## Diporphyrin Assemblies

This chapter features studies of di-porphyrin derivatives that have been introduced in section 1.2.1 (figure 1.1). Attached to the coplanar di-porphyrin core are six side-groups. The four 3,5-di(*tert*-butyl)phenyl moieties act as a spacer between the metal substrate and the porphyrin cores. This guarantees the porphyrin cores to be mostly decoupled from the metal surface. Furthermore these 'legs' seem to be relevant for the mobility of the molecules once adsorbed on the metal surface [54]. The two molecules used here only slightly differ in the details of the two other functional groups (figure 3.1). The first molecule which for convenience we call DDP features two 3-cyanophenyl moieties. In contrast, the other molecule has two 4-cyanophenyl groups attached. The cyano residue in the latter is located in the *para* conformation as opposed to the DDP where the cyano is attached in the *meta* conformation. Thus the second molecule will be distinguished by calling it pDDP. This chapter is focused mainly on two aspects of fullerene-porphyrin assemblies. First, the role of the cyanophenyl groups on the behavior of self-assembly of these molecules will be examined. And secondly it will be established that porphyrin monolayers are a suitable choice for creating structured surfaces which host fullerenes.

### 3.1 DDP Assemblies on Ag(100)

Approximately one ML of DDP has been deposited onto a clean Ag(100) substrate as described in sections 2.2.1 and 2.2.2. STM studies of DDP molecules adsorbed on this surface revealed a self-assembled layer as depicted in figure 3.2. Individual molecules can be clearly distinguished. The protrusions resulting from the molecules form fairly close packed rows. Each molecule is producing four lobes arranged in a roughly rectangular shape. The center to center distance of the lobes of one molecule was measured to be approximately 1.1 Å and 0.8 Å respectively. These distances are consistent with the expected distances between the 3,5-di(*tert*-butyl)phenyl substituents indicated in figure 3.3b. In accor-

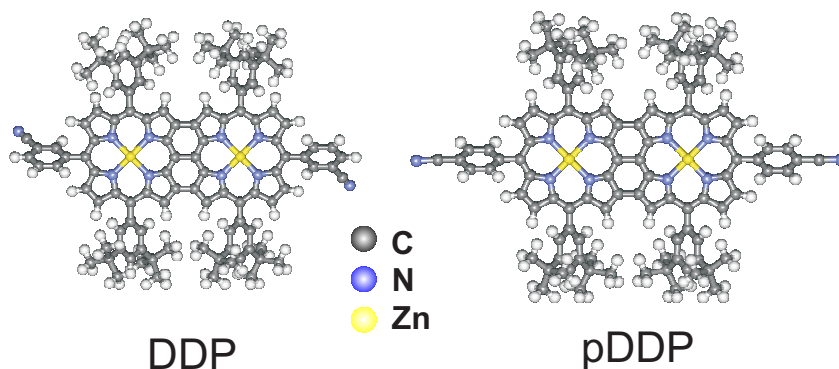


Figure 3.1: Structures of the di-porphyrin molecules described in this chapter. While DDP features two 3-cyanophenyl moieties (left, angled) the pDDP instead has two 4-cyanophenyl groups (right, straight) attached.

dance with this observation, earlier experiments conducted on similar porphyrins have also shown preferential tunneling transport through the di(*tert*-butyl)phenyl substituents [66–68]. Although the rotation of the 3,5-di(*tert*-butyl)phenyl substituents around the phenyl-porphyrin  $\sigma$ -bond is sterically hindered at small interplanar angles, they still have a certain degree of freedom to partially rotate without affecting each other. Therefore, the four protrusions appear with distinct heights due to a different conformation being adopted by the four 3,5-di(*tert*-butyl)phenyl moieties [67]. The cyanophenyl moieties did not show up on STM images at RT [69]. The distances between neighboring molecules of the ordered phase have been measured to be  $2.2 \pm 0.1$  nm in the direction labelled  $X_{DDP}$  and  $2.3 \pm 0.1$  nm in the direction  $Y_{DDP}$ . The two axes form an angle of  $120 \pm 5^\circ$ . The structure is rotated by  $\approx 7.5^\circ$  in respect to the [110] direction of the metal surface.

Considering all these findings, the model for this ordered monolayer is proposed as depicted in figure 3.3. It is important to note that the angle of the di(*tert*-butyl)phenyl with respect to the porphyrin core can not be determined from the STM data. However, the porphyrins seem to adopt into two distinctly different positions as evidenced from the two apparent heights in the STM images. Since the cyanophenyl moieties do not show up in the STM data it is also not clear which conformation these moieties adopt in the model. Most likely they favor one of the two following positions. First, the cyanophenyl ring might be oriented roughly perpendicular to the porphyrin core with the cyano group pointing down towards the silver atoms. N-donor ligands have been shown to form complexes with silver and thus enabling self-assembly in solution [70]. The interaction between the cyano groups and the silver substrate could be responsible for the stabilization of the self-assembled layer. Another possible interaction are hydrogen-bonds (H-bonds) formed with neighboring molecules. In order to

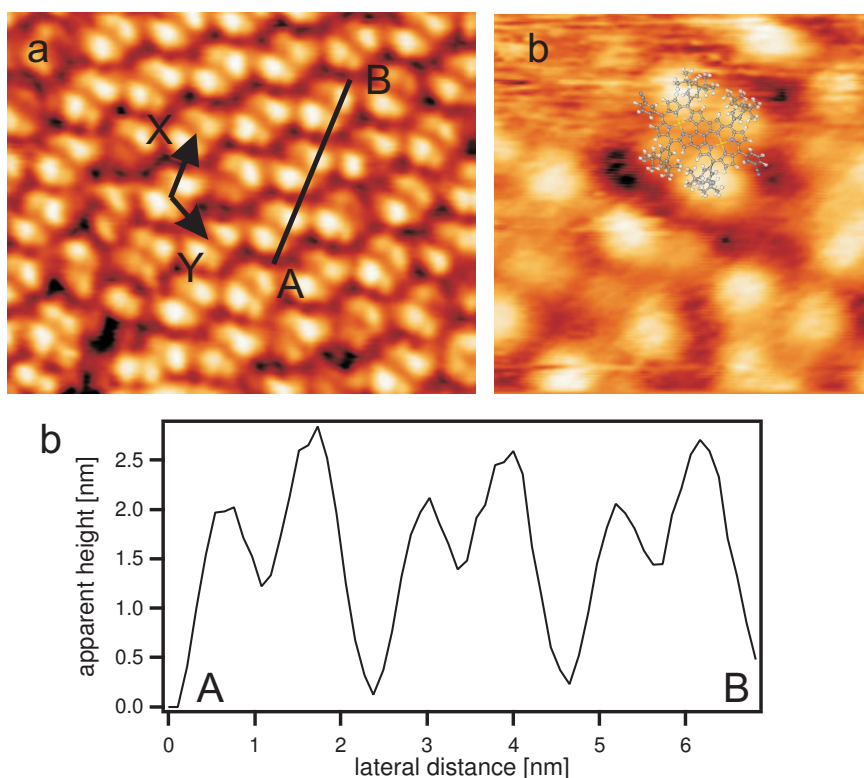


Figure 3.2: DDP molecules adsorbed on Ag(100). a) STM image of an ordered ML of DDP molecules (scan range:  $16 \times 13 \text{ nm}^2$ ,  $V_{bias} = 2.5 \text{ V}$ ,  $I_t = 72 \text{ pA}$ ,  $T = 298 \text{ K}$ ). The arrows indicating the distance from the center of a DDP molecule to the adjacent molecule (unit cell) are  $2.2 \pm 0.1 \text{ nm}$  and  $2.3 \pm 0.1 \text{ nm}$  long, enclosing an angle of  $120 \pm 5^\circ$ . b) Detailed STM image of DDP molecules (scan range:  $5 \times 5 \text{ nm}^2$ ,  $V_{bias} = 2.57 \text{ V}$ ,  $I_t = 21 \text{ pA}$ ,  $T = 298 \text{ K}$ ). The submolecular resolution shows four protrusions per DDP molecule caused by the 3,5-di(tert-butyl)phenyl substituents. c) Line section as indicated in image a. Clearly the protrusions exhibit two distinct apparent heights indicating different adsorption geometry of the respective legs.

allow for this, the cyanophenyl moieties have to adapt a small angle relative to the porphyrin plane. However, this is energetically not favorable due to the steric repulsion between the hydrogen atoms of the porphyrin core and the phenyl ring.

To better understand this self-assembly mechanism it is also interesting to take a look at an STM image taken at sub-ML coverage. Figure 3.4 was taken at a coverage of about 0.5 ML DDP. In the lower part of the image, one can see an ordered island. The remainder consists of horizontal streaks which are indicative of molecules moving with a speed comparable with the STM scan speed [39]. Also note that the image seems 'streaky' even on top of the ordered phase, indicating that molecules can move in spite of the emerging 2D ordering (maybe to some extent introduced by the STM tip). A similar 2D gas phase has been reported

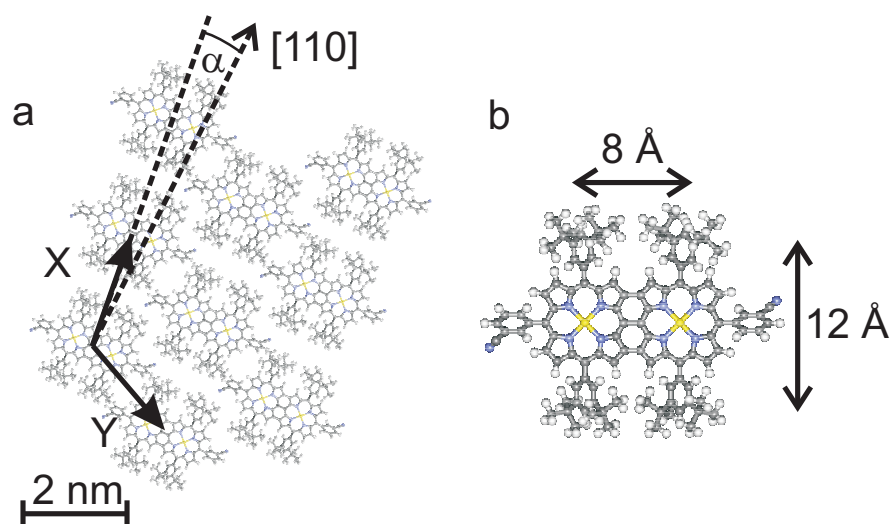


Figure 3.3: a) Proposed model of DDP molecules adsorbed on Ag(100). For clarity, all di(tert-butyl)phenyl are drawn with the same angle towards the porphyrins. However, STM images suggest that the groups adopt two different conformations. b) Relevant distances between the di(tert-butyl)phenyl substituents in a DDP.

for sub-ML coverage of phthalocyanine molecules on metals before [39, 71, 72]. Furthermore, in consecutive STM images one can observe the ordered island continuously growing/shrinking at the edges. This is attributed to the 2D solid-gas phase being in thermal equilibrium while continuously exchanging molecules between the condensed phase (ordered structure) and the gas phase. The ability of the molecules to move after being adsorbed on the surface is vital in order that they can assemble into ordered structures. If the intermolecular interaction is too weak to form stable ordered phases at sub-ML coverage, increasing the coverage to about 1.0 ML often triggers a condensation into the ordered 2D phase. In the case of this system increasing the DDP coverage induces the formation of large ordered domains.

## 3.2 pDDP Assemblies on Ag(100)

In order to evaluate the relevance of the attached functional groups on the 2D ordering we also investigated the pDDP molecule. This molecule consists of exactly the same atoms as DDP but the cyanophenyl group is located in the para position as described at the start of this chapter. All other experimental parameters and the substrate were kept the same.

Figure 3.5 shows STM images acquired after evaporation of  $\approx 1.0$  ML pDDP onto a clean Ag(100) surface. Again, each diporphyrin molecule was imaged as

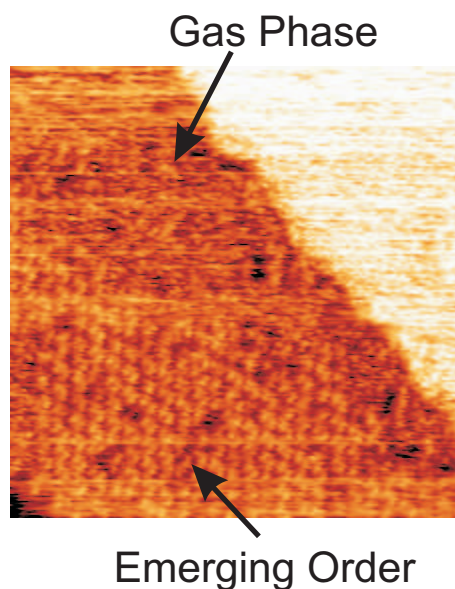


Figure 3.4: STM image (scan range:  $50 \times 50 \text{ nm}^2$ ,  $V_{bias} = 0.9 \text{ V}$ ,  $I_t = 30 \text{ pA}$ ,  $T = 298 \text{ K}$ ) showing ordered structure right next to mobile molecules (gas phase) of DDP on Ag(100). The ordered 2D phase and the gas phase adopt a thermal equilibrium with constantly changing borders.

four protrusions. Interestingly, all di(tert-butyl)phenyl moieties were recorded to have the same apparent height as evidenced in the linecut in figure 3.5c. The four protrusions appear to form a rhombic shape indicated by D in 3.5b. The distance between neighboring molecules are  $X_{pDDP} = 1.9 \pm 0.1 \text{ nm}$  and  $Y_{pDDP} = 2.2 \pm 0.1 \text{ nm}$  with an enclosed angle of  $120 \pm 5^\circ$ .

The model in figure 3.6a takes all these observations except the rhomboid appearance into account. This distortion can be explained by assuming that not all 3,5-di(tert-butyl)phenyl groups are rotated in the same direction as is the case in DDP. Instead the four 3,5-di(tert-butyl)phenyl substituents adopt a 'crossed leg' conformation as depicted in figure 3.6c. A very similar observation has been made by Kuntze et al. after deposition of lander molecules onto Cu(100) [73] where both the 'parallel leg' and the 'crossed leg' conformation could be observed. In our case the legs would have to be tilted by about  $30^\circ$  both in the direction which is allowed by the  $\sigma$ -bond as well as in the direction perpendicular to this bond, probably by deformation of the porphyrin core. These values are comparable to the angles measured in the case of the lander molecules.

However, there is a second possibility. While we are fairly certain about the fact that the di(tert-butyl)phenyl groups are responsible for the observed protrusions, it is not immediately evident which four protrusions should be picked

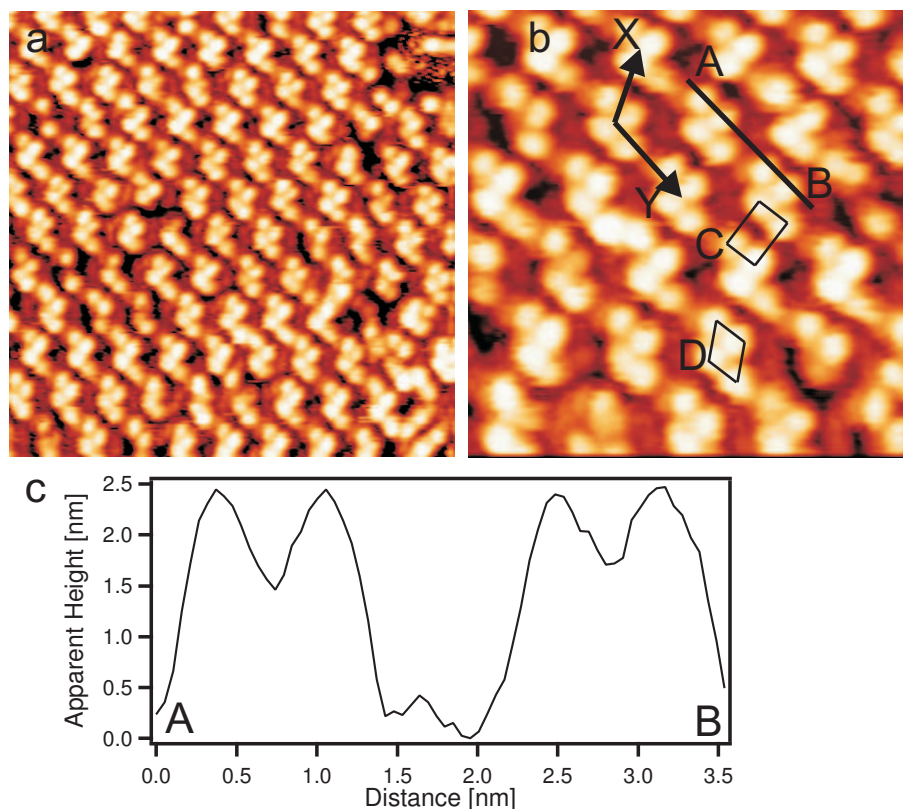


Figure 3.5: a) Overview STM image (scan range:  $20 \times 20 \text{ nm}^2$ ,  $V_{bias} = 2.86 \text{ V}$ ,  $I_t = 13 \text{ pA}$ ,  $T = 298 \text{ K}$ ) of a ML of pDDP on Ag(100). b) Detailed STM image (scan range:  $10 \times 10 \text{ nm}^2$ ,  $V_{bias} = 2.86 \text{ V}$ ,  $I_t = 13 \text{ pA}$ ,  $T = 298 \text{ K}$ ) showing submolecular resolution of the pDDP molecules. The distance between two centers of molecules are  $1.9 \pm 0.1 \text{ nm}$  and  $2.2 \pm 0.1 \text{ nm}$  along the X and Y directions respectively (indicated by arrows). These enclose an angle of  $120 \pm 5^\circ$ . The two possibilities to connect the protrusions (signifying di(*tert*-butyl)phenyl legs) are indicated by C and D. c) Line section along the line indicated in b (from A to B) showing that the protrusions feature the same apparent height.

to form one molecule. Most of the time the four protrusions which belong together can be identified by observation of a deeper 'valley' between the protrusions of adjacent molecules (e.g. section 3.1 and 4.3). Other times, this rule of thumb is not valid as in section 4.2. Fortunately, the respective distances between the lobes usually clarifies the matter. However, this is not the case in this instance. If one connects the protrusions as indicated by C in 3.5b the resulting ordering can be explained without bending of the di(*tert*-butyl)phenyl legs. Another argument in favor of this second model (figure 3.6d) is the position of the cyano residues. Whereas the first model would indicate two cyano moieties facing each other (which seems unlikely) the second model would have the cyano groups shifted in respect to each other. The rigid para-cyanophenyl groups feature a distance of a couple of Å to the di(*tert*-butyl)phenyl legs in this model which allows for



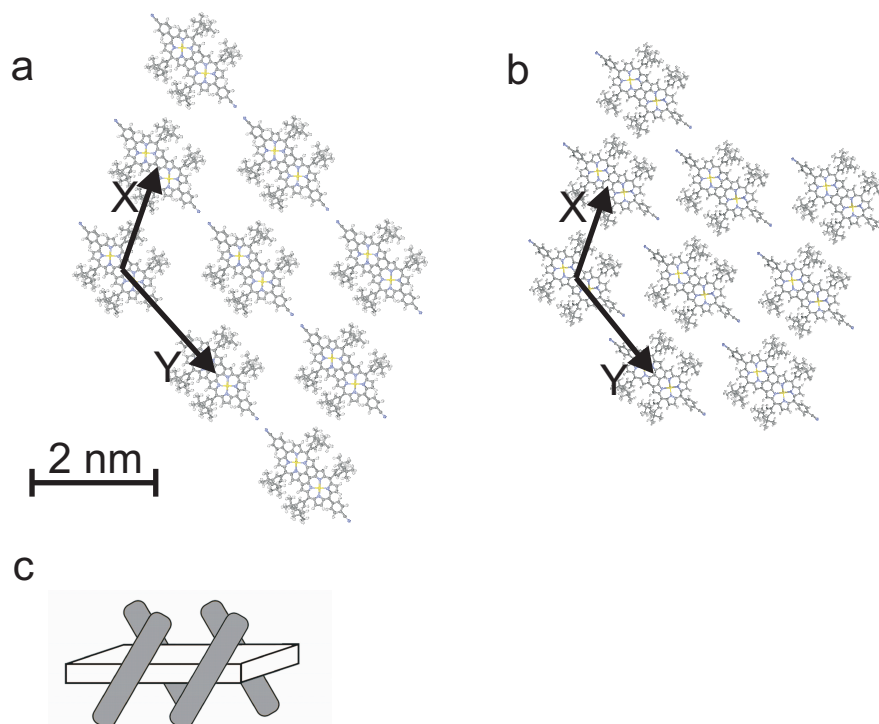


Figure 3.6: Proposed model for pDDP molecules adsorbed on Ag(100). a) Model one, assuming the 'crossed leg' conformation as depicted in c. b) Model without the 'crossed leg' conformation. For geometric reasons the lattice constants ( $X$  and  $Y$ ) and the enclosed angle possess the same values in both models, slightly rotated compared to each other. c) Cartoon visualizing the 'crossed leg' conformation. The grey di(tert-butyl)phenyl legs are tilted at about  $30^\circ$  in respect to the porphyrin plane.

interaction via H-bonding. Of course, the values for  $X_{pDDP}$ ,  $Y_{pDDP}$  and angle stay the same in this model.

### 3.3 The Importance of the Functional Groups for the Self-Assembly

The results of the previous two chapters show that the functional groups attached to the molecules influence the self-assembly mechanism. This is perhaps most obvious when one compares the area one molecule occupies in these ordered structures. While the DDP structure uses an area of  $4.4 \text{ nm}^2$  per molecule the pDDP structure needs only  $3.6 \text{ nm}^2$  per molecule on the same substrate. This is an amazing difference of almost 20% considering that only the position of the cyano group has been changed with the rest of the molecule unchanged and the same substrate. Looking at the models one might counter that the geometrical

alignment seems to be rather similar. However, this fact is attributed to being a substrate induced property, as will be discussed in detail in section 4.4.

In order to further investigate the role of the cyano residues for the self-assembly additional experiments were conducted with di-porphyrin molecules featuring only di(*tert*-butyl)phenyl substituents. Unlike the DDP or pDDP, these molecules did not have a cyanophenyl group attached but instead had an additional two di(*tert*-butyl)phenyl legs in their place. Deposition of these molecules did not result in the formation of any ordered structures, neither on Ag(100) nor on Ag(111) for any coverage up to 1ML. Instead, STM images (not shown in this work) of the disordered molecules exhibit areas of noisy spikes indicative of mobile molecules throughout the whole surface. Obviously the interaction between the cyano substituents and the molecule and/or substrate is required to form the ordered porphyrin layers. Combining this knowledge with the observation of mobile phases next to ordered phases (e.g. figure 3.4) one can deduct that most likely interactions between the cyanophenyl moieties and neighboring molecules are responsible for the ordering. Due to the polarity of the cyano (electronegativity C=2.55, N=3.04 (Pauling scale)) and C-H groups (electronegativity C=2.55, H=2.20) H-bonds can be formed between these groups. The structure of the porphyrins used in this study offer various hydrogen atoms in different positions as possible interaction counterparts to the cyano moieties. H-bonds with C-H groups as donors generally form weak bonds with interaction energies of about 17-170 meV (usually  $< 87$  meV) [74]. Furthermore, such weak H-bonds do not need to be exactly aligned along the C-H and C $\equiv$ N bonds but can feature an angle of up to 70° [74]. Furthermore, it is important to note that the adsorbed molecules on a surface generally favor discrete adsorption sites (e.g. top sites). Due to this and the fixed length of the covalent bonds, the H-bond may not be able to achieve the optimal distance and thus feature even weaker interaction energy.

### 3.4 C<sub>60</sub> - DDP Assemblies on Ag(100)

Sublimation of  $\approx 0.02$  ML of C<sub>60</sub> on top of a preformed monolayer of DDP on Ag(100) resulted in the predominant formation of unidirectional chains of various lengths composed of several bright protrusions (Figure 3.7). Furthermore, chains consisting of a maximum of three C<sub>60</sub> molecules tilted at an angle of  $120 \pm 4^\circ$  with respect to the main direction of the fullerene chains have been observed. The protrusions feature an apparent height of about  $4.4 \pm 0.2$  Å measured with respect to the porphyrin layer and a diameter of roughly 1.5 nm. Even though the vdW diameter of C<sub>60</sub> is only ca. 1 nm, the observed diameter of 1.5 nm can easily be accounted for by the broadening of the peak by the tip convolution.



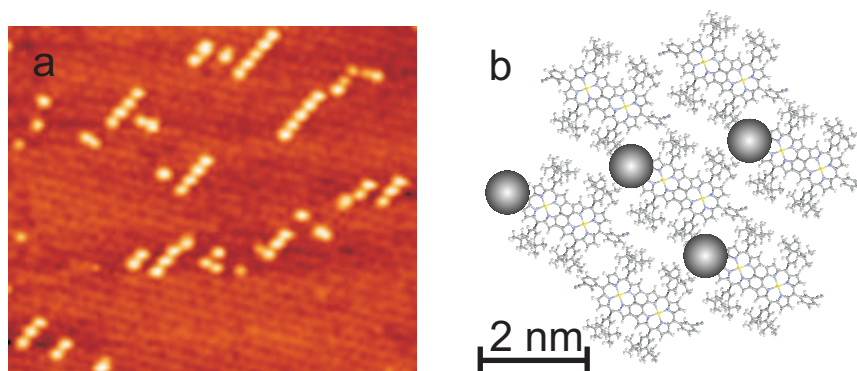


Figure 3.7: C<sub>60</sub> - DDP assemblies on Ag(100). a) STM image (scan range:  $77 \times 65 \text{ nm}^2$ ,  $V_{bias} = 2.59 \text{ V}$ ,  $I_t = 22 \text{ pA}$ ,  $T = 298 \text{ K}$ ) showing the preferential direction of the chainlike assembly of C<sub>60</sub> on a previously deposited monolayer of DDP molecules. b) Proposed model for the adsorption of C<sub>60</sub> on DDP as deduced from the detailed images (figure 3.8)

With their spherical appearance in the STM data these protrusions can clearly be identified as the C<sub>60</sub> molecules. The longest chains ( $\approx 15.5 \text{ nm}$ ) are composed of eight C<sub>60</sub> molecules with an intermolecular C<sub>60</sub>-C<sub>60</sub> distance of about 2.2 nm. Surprisingly, no 2D islands composed of C<sub>60</sub> have been found. The superstructure of the bimolecular C<sub>60</sub>-DDP assembly (figure 3.7) which best fits the experimental data is also depicted (figure 3.7b). Despite the large surface area of the fused macrocyclic core (ca.  $1 \text{ nm}^2$ ), the fullerene-based chains are formed by molecules which are located outside of the porphyrin macrocycles, precisely on top of the 3-cyanophenyl substituents.

To exclude the possibility that the C<sub>60</sub> molecules are embedded in the porphyrin domains as self-intermixed phase - such as in subphthalocyanine and C<sub>60</sub> assemblies [75], for example - single-molecule repositioning experiments of the fullerenes were performed. Figure 3.8 shows the STM images recorded before (left) and after (right) C<sub>60</sub> repositioning on a full monolayer of DDP. After the relocation sequence, the former fullerene site (green ellipse in Figure 3.8b) is clearly occupied only by DDP, thus proving that the C<sub>60</sub> molecules sit on top of the monolayer. Interestingly all attempts toward the formation of square islands composed of four carbon spheres failed. Instead those experiments led to the abstraction of a C<sub>60</sub> molecule, as evident with the fullerene molecule positioned at the end of the left chain (blue circle in Figure 3.8). The latter observation hints at an intrinsic property of such layers of DDP: condensed 2D phases composed of C<sub>60</sub> molecules are energetically unfavored and only chainlike phases are preferred.

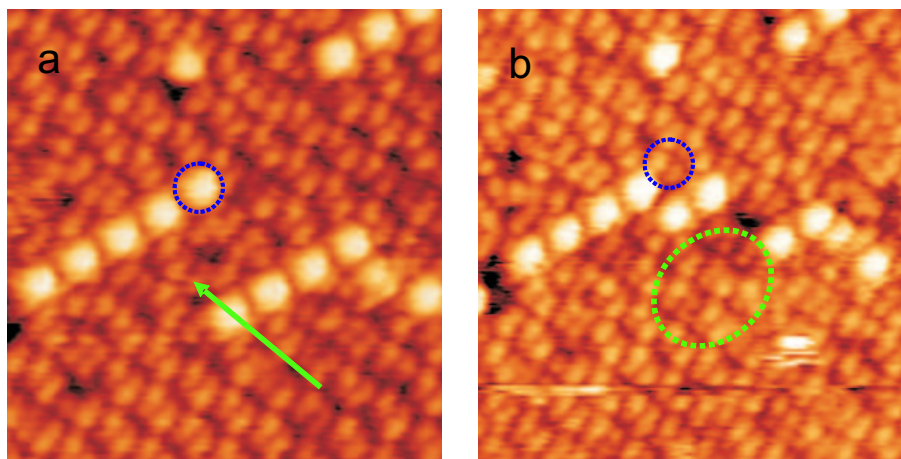


Figure 3.8: STM image of  $C_{60}$  manipulation sequence. STM images before (a) and after (b) manipulation (scan range:  $21 \times 21 \text{ nm}^2$ ,  $V_{bias} = 1.43 \text{ V}$ ,  $I_t = 11 \text{ pA}$ ,  $T = 298 \text{ K}$ ) of the  $C_{60}$  molecule adsorbed on the DDP layer. The green arrow indicates the path of the STM tip during the manipulation (tunneling parameters:  $I_t = 214 \text{ pA}$ ,  $V_{bias} = 1.43 \text{ V}$ ,  $V_{tip} = 5 \text{ nms}^{-1}$ ). The green ellipse indicates the intact layer of DDP molecules after repositioning of the  $C_{60}$  molecules. One  $C_{60}$  molecule vanished during the repositioning experiment (blue circle).

The  $C_{60}$  molecules do not diffuse on the DDP layer at RT. This observation indicates that the energy barrier for diffusion of the  $C_{60}$  molecules is larger than the thermal energy at 298 K. The large  $C_{60}$ - $C_{60}$  distance in the superstructure excludes the presence of any significant contribution from the cohesive  $C_{60}$ - $C_{60}$  energy, which is of the order of 1.7 eV at a separation of about 1 nm [76]. Moreover, in agreement with previous studies in solution [77], any strong fullerene-porphyrin interactions are absent in the assembly of DDP, since the  $C_{60}$  molecules are not located directly above the macrocyclic cores and can be repositioned without altering the underlying porphyrin layer.

### 3.5 Upside Down: Porphyrin deposition on $C_{60}$ Monolayers

In order to better understand the interaction between adsorbed fullerene and adsorbed porphyrin molecules the order of deposition was reversed. First, a sub-ML of  $C_{60}$  molecules was evaporated onto the clean Ag(111) substrate. As remarked in section 1.2.2 the adsorption and self-assembly of  $C_{60}$  monolayers has been well studied. In accordance to those studies deposition of  $\approx 0.5 \text{ ML}$  lead to self-assembled  $(2\sqrt{3} \times 2\sqrt{3})R \pm 30^\circ$  fullerene domains predominantly located along the step edges of the silver substrate. Subsequent deposition of  $\approx 0.5 \text{ ML}$  DDP molecules resulted in the disordered adsorption as depicted in figure 3.9a. On the

bottom right hand side of the STM image one can clearly see some single diporphyrin molecules while on the bottom left they seem to aggregate and can not be identified easily. Furthermore, streaks on top of the  $C_{60}$  monolayer as well on the previously empty metal indicate the presence of many mobile DDP molecules. Several molecules are only half imaged which indicates that the influence of the STM tip may laterally displace the molecules in the fast scan direction even while using scanning parameters with high tunneling resistance [78].

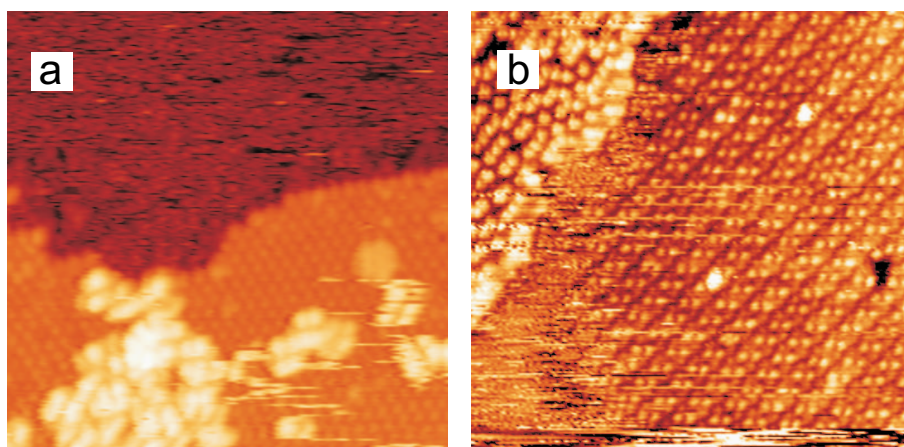


Figure 3.9: STM images of DDP molecules deposited on preadsorbed  $C_{60}$  ML. a) STM image (scan range:  $30 \times 30 \text{ nm}^2$ ,  $V_{bias} = 2.50 \text{ V}$ ,  $I_t = 15 \text{ pA}$ ,  $T = 298 \text{ K}$ ) showing DDP molecules (bright, lower part) on top of an ordered  $C_{60}$  ML (hexagonal close packed). The DDP molecules are rather mobile (streaks and half molecules) indicating a weak interaction between the two layers. The upper half of the image consists of mobile porphyrins (gas phase) on the metal substrate. b) STM image (scan range:  $42 \times 42 \text{ nm}^2$ ,  $V_{bias} = 2.80 \text{ V}$ ,  $I_t = 12 \text{ pA}$ ,  $T = 298 \text{ K}$ ) after thermal annealing to  $450 \text{ K}$ . Most molecules have separated into pure  $C_{60}$  and DDP domains. A few scattered  $C_{60}$  molecules can be found on top of the porphyrin layer.

Thermal annealing to  $450 \text{ K}$  of the assembly shown in figure 3.9a results in a complete phase separation (figure 3.9b). In the upper left corner the  $C_{60}$  molecules form disordered islands. The DDP molecules assemble into an ordered layer. Only a few  $C_{60}$  molecules can be found on top of the ordered porphyrin structure where they seem to be immobile.

From these observations we conclude that the interaction of the porphyrins adsorbed on  $C_{60}$  layers is weaker than in the case of  $C_{60}$  on top of porphyrin layers described in section 3.4. The interaction with the metal surface seems to be relevant for the ordering of the porphyrins. Even though  $C_{60}$  are electron acceptors and porphyrins are electron donors not much interaction can be observed. One reason for this could be the well know charge transfer between the metal substrate and the fullerenes. Having already accepted more than two electrons

per molecule [24] the  $C_{60}$  electron accepting capability might be saturated. The conducted experiments indicate that the interaction between the porphyrin core and the  $C_{60}$  are not relevant to the formation of these guest-host systems. The following experiments with monoporphyrim derivatives will only confirm these findings.

# Chapter 4

## Monoporphyrin Assemblies

The molecules used in this chapter differ from those presented before in that they are built from only one porphyrin moiety and have only four side groups attached. Again the molecules feature two 3-cyanophenyl moieties. However in this case only two 3,5-di(tert-butyl)phenyl groups are used as spacer legs (figure 4.1). These molecules will be referred to as DMP. The aim of this chapter is to discuss the influence the substrate plays in the self-assembly process of DMP molecules and to show the new exciting structured surfaces which were produced, most notably a porous network hosting fullerenes and the paired  $C_{60}$  structures to be introduced in section 4.6.

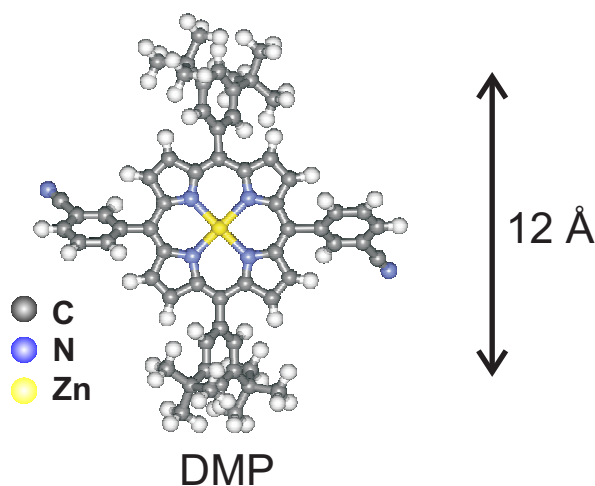


Figure 4.1: Structure of the mono-porphyrin molecules used in this chapter. Each porphyrin features two 3,5-di(tert-butyl)phenyl and two 3-cyanophenyl moieties.

## 4.1 DMP Assemblies on Ag(100)

DMP molecules were sublimed onto a Ag(100) surface. Analogous to the DDP and pDDP molecules, the DMP molecules can be observed both as a 2D gas phase and in the form of ordered islands at sub-ML coverage. Again only the di(tert-butyl)phenyl groups can be imaged in STM images (figure 4.2), producing two bright protrusions per molecule. All the legs show up with the same apparent height of about 1.8 nm suggesting that all the di(tert-butyl)phenyl moieties are adsorbed equivalently and featuring the same angle in respect to the porphyrin cores. The distance between two protrusions was measured to be about 1.1 nm. This compares well with the theoretical value of 12 Å measured for the distance between two di(tert-butyl)phenyl legs (figure 4.1). The intermolecular distances in this monolayer are  $X_{DMP1} = 2.4 \pm 0.1$  nm and  $Y_{DMP1} = 1.5 \pm 0.1$  nm. The two axes form an angle of  $126 \pm 5^\circ$ . The  $X_{DMP1}$  axis is parallel to the [110] direction of the silver substrate within the accuracy of the STM measurements.

## 4.2 DMP on Cu(111)

Deposition of DMP molecules onto a Cu(111) surface resulted in the formation of the two ordered phases depicted in figure 4.3a and b. The lower right corner features a close-packed structure looking as if the molecules are arranged in rows. The image of this ordering is built from groups of four bright protrusions arranged in a linear structure. The other phase consists of rows of holes each surrounded by six protrusions. Notably, these are not distributed with regular spacing. Instead, there are two groups of two protrusions sitting close to each other with a distance comparable to the one seen in the groups of four of the close-packed phase. The other two single dots are distanced distinctly farther from the neighboring protrusions. It is interesting to note that in between two rows of holes one can always observe one or more rows of the four-protrusion-groups characteristic for the close-packed phase.

If one analyzes the distances between the four protrusions of the close packed phase, which again mark the di(tert-butyl)phenyl legs, it turns out that these groups cannot be made up by two molecules. The distances are too small for this possibility. However, the distance from the corner of one group to the next group of four nicely fits the expected intramolecular distance of 12 Å. Figure 4.4a depicts the resulting tentative model. The surface is thus covered with DMP molecules adsorbed with two distinct rotations. These are arranged into rows of alternating rotated molecules. In order to guide the eye, two groups of protrusions are marked by red circles. Indeed, one group of four protrusions is produced from one leg each of four different molecules.



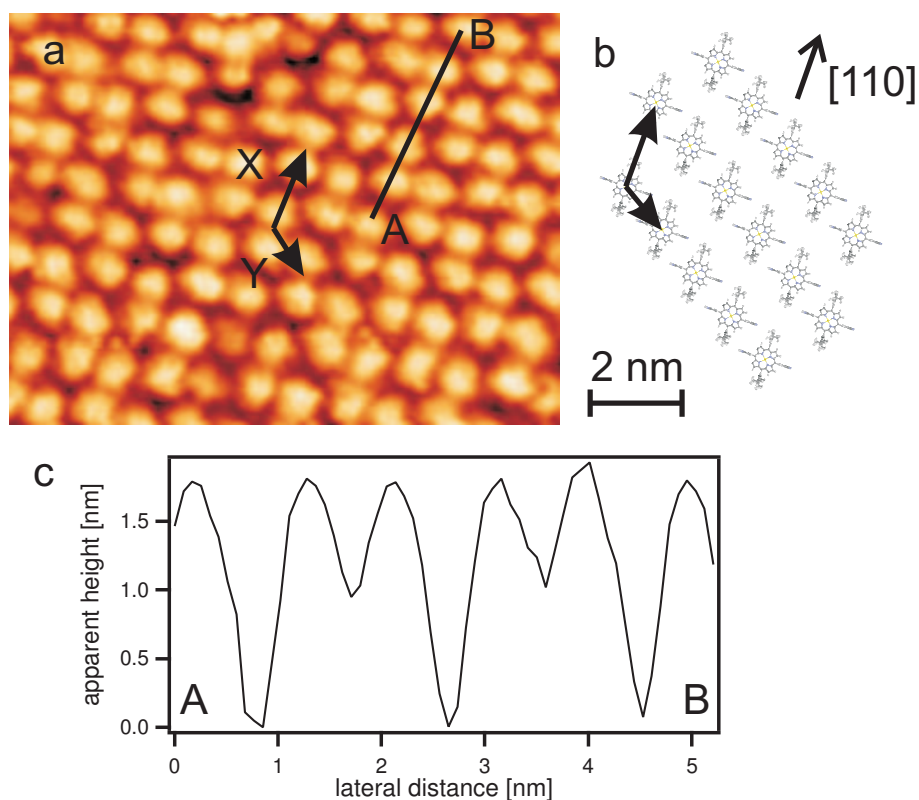


Figure 4.2: a) STM image (scan range:  $12 \times 9 \text{ nm}^2$ ,  $V_{bias} = 2.8 \text{ V}$ ,  $I_t = 72 \text{ pA}$ ,  $T = 298 \text{ K}$ ) of a ML of DMP on Ag(100). The distance between the centers of two neighboring molecular subunits is  $2.4 \pm 0.1 \text{ nm}$  and  $1.5 \pm 0.1 \text{ nm}$  enclosing an angle of  $126 \pm 5^\circ$  as marked by arrows. b) Proposed model of the self-assembled ML of DMP on Ag(100). The molecules are arranged along the [110] direction of the underlying substrate. c) Line section from A to B as marked in a. All protrusions show the same apparent height indicating that all di(tert-butyl)phenyl legs are adsorbed equivalently.

Starting from the model of the close-packed ordering it is straight forward to deduct the positions of the molecules around the holes. Since only one di(tert-butyl)phenyl group of each molecule belongs to the group of four, most of the protrusions surrounding a hole are identified at once. This leaves only two points to connect. Unsurprisingly, the distance is exactly the expected distance between two of the legs. Figure 4.4b shows the resulting model. The holes emerge from the fact that one molecule is turned the 'wrong way' compared to the close-packed ordering. This prevents two molecules from taking their respective positions. Interestingly, this molecule does not feature a completely new orientation but rather one of the orientations already found in the close-packed phase. Because this molecule contributes one protrusion to two different holes a line of holes can only be stopped by a defect in the ordering as observed in figure 4.3a (lowest row of holes, right side of the image). To visualize the ordering around a hole

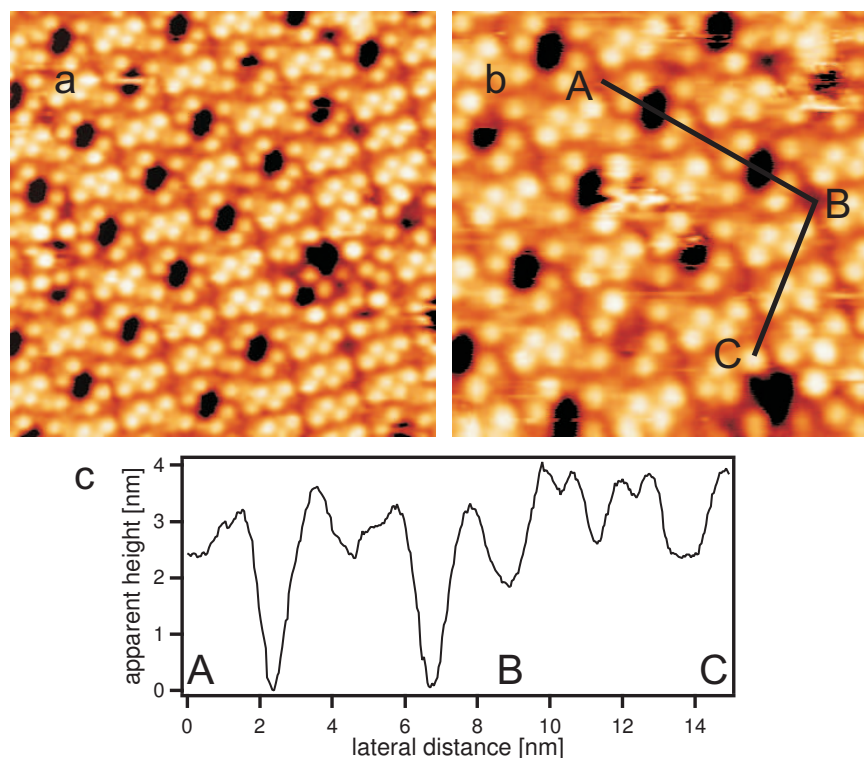


Figure 4.3: STM images of DMP on Cu(111). a) Overview image (scan range:  $22 \times 22 \text{ nm}^2$ ,  $V_{bias} = 2.97 \text{ V}$ ,  $I_t = 23 \text{ pA}$ ,  $T = 298 \text{ K}$ ) showing the close-packed phase (lower right corner) and rows of holes with varying row to row distance. b) Detailed STM image (scan range:  $22 \times 22 \text{ nm}^2$ ,  $V_{bias} = 2.97 \text{ V}$ ,  $I_t = 22 \text{ pA}$ ,  $T = 298 \text{ K}$ ) of part of the area depicted in a. Submolecular resolution allows us again to identify the protrusions produced by tunneling through the di(tert-butyl)phenyl groups. c) Line section (as indicated in b) showing two pores (A to B) and close-packed phase (B to C). The protrusions between B and C feature the same apparent height indicating that all legs are adsorbed with the same configuration. The apparent height at pores only seems to be different because the section is not exactly running through the center of the protrusions.

the actual positions of the protrusions around two of the holes are marked with red circles recreating the characteristic arrangement observed in the STM images. For comparison, the missing protrusions of one hole are marked with green circles (figure 4.4b).

Examination of all the STM images of DMP on Cu(111) revealed rather large areas covered only with the close-packed phase next to large areas of the hole ordering. Furthermore the rows of holes can be spaced at different intervals, as opposed to featuring a reoccurring pattern of distances. Both these observations indicate that the occurrence of these intermixed phases are not related to reducing stress based on lattice mismatch of either phase relative to the substrate. More



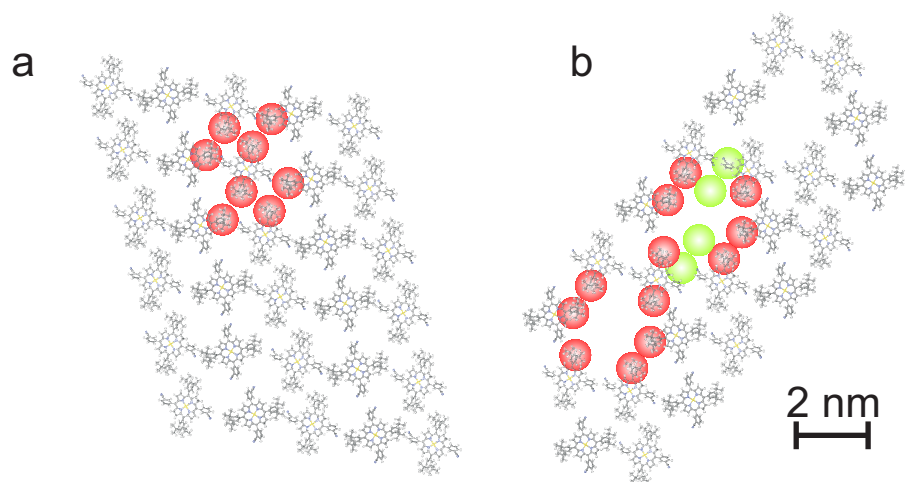


Figure 4.4: Model of DMP adsorbed on Cu(111). a) Model of the close-packed phase. The assembly consists of molecules adsorbed in two distinct angles arranged in rows. The four protrusions which seem to build a subunit in figure 4.3 actually consist of four molecules each contributing one di(*tert*-butyl)phenyl group. In order to guide the eye, two of those groups are highlighted by red dots. b) Model of the pores. Between two pores one molecule is adsorbed exhibiting a different rotation than expected from the close-packed phase, in turn preventing two molecules to adsorb where they would be (green dots). This leads to the distinctive aperiodic arrangement of the protrusions (indicated by red dots).

likely, the proportion of the two arrangements is due to the local and global density of DMP molecules.

### 4.3 DMP Assemblies on Ag(111)

Deposition of  $\approx 1$  ML of DMP on a Ag(111) substrate and subsequent annealing to  $\approx 450$  K resulted in the formation of a close packed layer of porphyrins as depicted in figure 4.5. The two protrusions representing a single DMP molecule order in molecular rows along the  $X_{DMP2}$  and  $Y_{DMP2}$  directions with molecule-molecule distances of  $1.8 \pm 0.1$  nm and  $3.3 \pm 0.1$  nm respectively. All protrusions appear with the same apparent height as can be seen in the line section (figure 4.5c).

At lower coverage of  $0.5 - 0.7$  ML DMP on Ag(111) the molecules formed a supramolecular network featuring hexagonally arranged pores (figure 4.6). The pore-pore distance was measured to be  $3.3 \pm 0.1$  nm. High resolution STM images such as the one in figure 4.6b show the two di(*tert*-butyl)phenyl legs with a distance of  $12 \text{ \AA}$  indicating the porphyrin derivatives are again adsorbed flat on the surface and are not overlapping each other. The assembly was found to

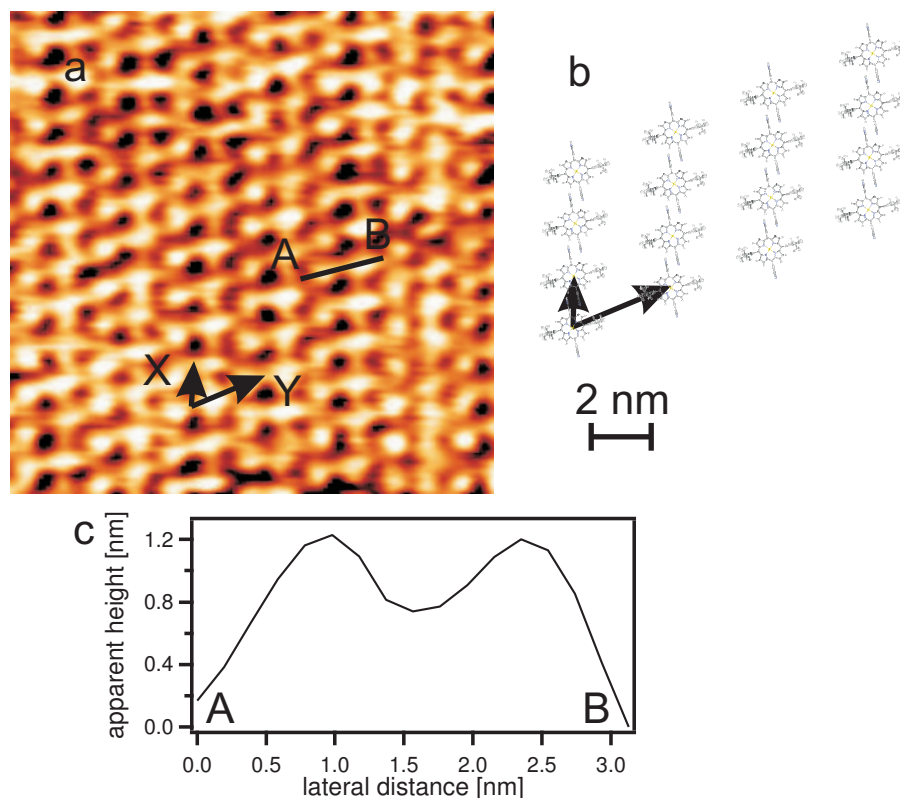


Figure 4.5: Close-packed assembly of DMP on Ag(111). a) STM image (scan range:  $21 \times 21 \text{ nm}^2$ ,  $V_{bias} = 2.78 \text{ V}$ ,  $I_t = 18 \text{ pA}$ ,  $T = 298 \text{ K}$ ) of the assembly resulting after annealing to 450 K. The distance between the centers of two neighboring molecular subunits is  $1.8 \pm 0.1 \text{ nm}$  and  $3.3 \pm 0.1 \text{ nm}$  along the two directions marked with the arrow. The molecular rows cross each other at an angle of  $92 \pm 4^\circ$ . b) Proposed model of the close-packed phase. c) Line section along the line (A, B) as indicated in a. All protrusions show the same apparent height.

be stable even after thermally annealing the sample with temperatures of up to 448 K. Figure 4.6c shows the cross-section through a pore with the typical pore characteristics of an apparent depth of  $\approx 1.2 \text{ \AA}$  and a pore diameter of  $\approx 1.2 \text{ nm}$ . These details are to be taken as minimal estimations, however. The finite size of the tip is expected to cause the pores to be imaged smaller in both lateral and vertical size than their real dimensions due to the tip-surface convolution. Compared to the [1-11] direction of the substrate surface the superstructure is rotated by  $\alpha = 15 \pm 4^\circ$  as depicted in figure 4.7. This self-assembled supermolecular monolayer covers large metal terraces with a nearly perfectly ordered porous network (see overview image in figure 4.6a). Particularly in close proximity to step edges the characteristic 2D gas phase can be seen. Again the border between condensed phase and 2D gas phase can be observed to fluctuate. In the detailed view (figure 4.7b) one single pore can be seen which is surrounded by three DMP molecules. All three porphyrins are arranged so that the 3-cyanophenyl moieties

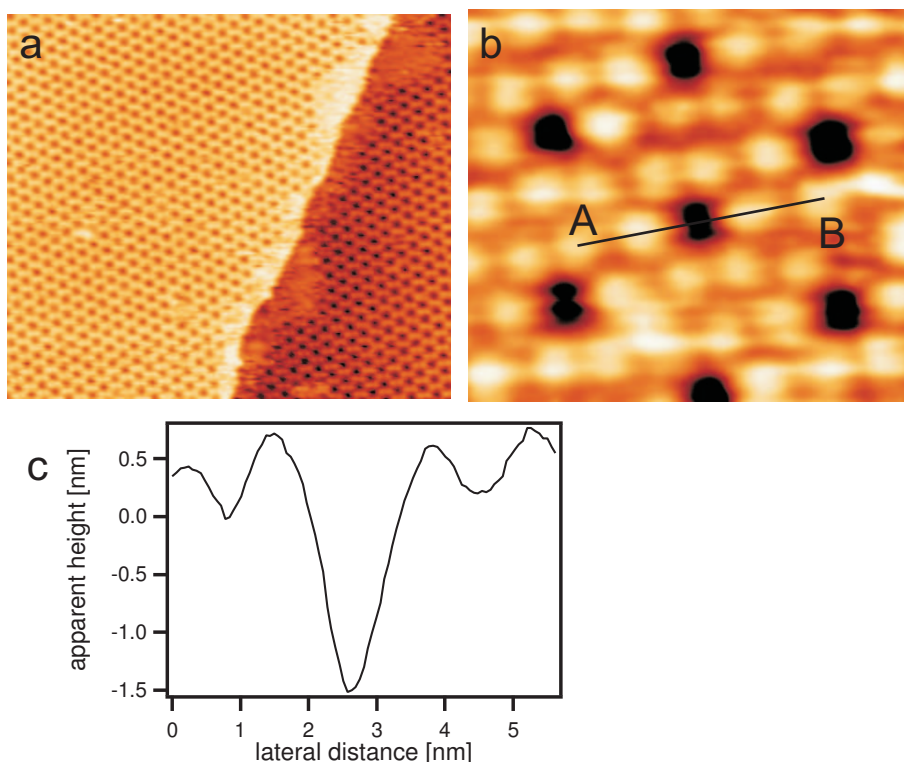


Figure 4.6: a) Overview STM image (scan range:  $96 \times 83$  nm<sup>2</sup>,  $V_{bias} = 3.00$  V,  $I_t = 15$  pA,  $T = 298$  K) of DMP molecules on Ag(111) self-assembled into a hexagonal porous network. Close to the step edge a small area of mobile 2D molecular gas phase can be observed. b) Detailed STM image (scan range:  $9 \times 8$  nm<sup>2</sup>,  $V_{bias} = 2.90$  V,  $I_t = 25$  pA,  $T = 298$  K) of the porous assembly. Each porphyrin molecule appears as two bright protrusions, which are separated by about 1.2 nm. The center-to-center distance between two neighboring pores is  $3.3 \pm 0.1$  nm. c) Line section profile of a single pore (from A to B).

point towards the pore resulting in the formation of trimeric units with a central cavity. Clearly the cyanophenyl groups here also play a crucial role for the self-assembly as established in the last chapter. Due to the rotational freedom around the  $\sigma$ -bond we propose two alternative mechanisms influencing the organization.

Firstly, the cyanophenyl groups may be located in their 'relaxed' gas phase position with the phenyl rings perpendicular to the porphyrin just as they are depicted in figure 4.7b. N-donor ligands such as these cyano residues have been shown to form coordination bonds with silver [70]. Thus the interaction between the cyanophenyl groups and the silver could help stabilize the organization of the structured monolayer.

The other possibility would be to turn the phenyl rings into a position roughly parallel to the porphyrin core. Even though the conformation with the phenyl

rings exactly parallel to the porphyrin seems unlikely due to steric repulsion between the attached hydrogen atom, an angle close to parallel could allow hydrogen bonds between one cyano and an adjacent phenyl ring. It has been noted (section 3.3 that hydrogen bonds do not require to be aligned precisely in a straight line, especially if the bond is of a rather weak nature [74]. Thus it seems plausible to expect the cyanophenyl moieties to form a cyclic arrangement of hydrogen bonds. Furthermore, the cyano residues which are pointing away from the pores possess an abundance of possibilities to form similar hydrogen bonds to one of the neighboring di(*tert*-butyl)phenyl groups. The best approximation of the distance between the cyclic cyano residues and between the cyano residues and the di(*tert*-butyl)phenyl legs possible from the available STM data are of the order of a few Å. This is in accordance to the expected distance for weak hydrogen bonds (bond length  $> 2.2$  Å) [74].

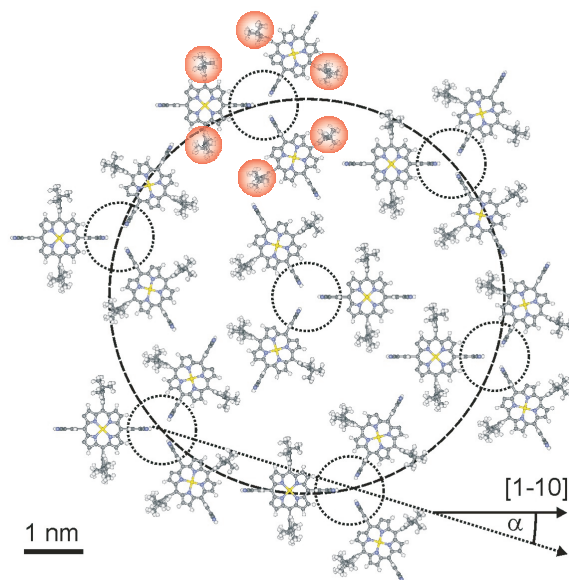


Figure 4.7: Proposed model of the porous DMP assembly on Ag(111). Each pore is surrounded by three DMP molecules with the cyanophenyl moieties pointing towards the center of the pore. The di(*tert*-butyl)phenyl legs imaged in STM measurements result in evenly spaced protrusions around the pore, as indicated by the red dots.

Time-lapsed images of the porous DMP layer (shown in the next chapter, figure 5.3) reveal that a certain conformational flexibility of the porphyrins is present. In figure 5.3a-c one can observe protrusions which change from dim to bright (and back) in the course of the measurement (indicated by colored arrows). Such molecular fluctuations can be attributed to rotational motion of the di(*tert*-

butyl)phenyl moieties and have been observed and investigated before [67, 68]. Another interesting feature of this monolayer is its capability to heal itself. This is also evidenced in the series of images in figure 5.3a-c. In image 5.3a one defect can be seen (marked by the ellipse) in the otherwise perfect ordering. The imperfection then starts to heal and propagate towards the border of the self-assembled layer during the subsequent images.

## 4.4 The Importance of the Substrate for the Self-Assembly

In chapter 3.3 it was shown that variation of the functional groups of the molecules strongly influences the ordering of the resulting molecular layer. The three preceding sections clearly show that the ordering of the molecules is also influenced by the choice of substrate. The resulting ordering seems to be an interplay between both factors. It stands to reason that a surface consisting of different metal atoms (e.g. silver or copper) exert dissimilar effects on the molecules. However, even the crystal direction of the metal surface (e.g. Ag(100) or Ag(111)) plays an important role in determining the resulting assembly. One can think of many causes for the different behavior such as the size of the constituent metal atoms, their chemical reactivity, different work functions, etc. In addition to molecule-surface interactions, molecule-molecule interactions are relevant to the resulting ordering (or lack thereof) of the molecules. This multitude of possible parameters introduces high complexity, currently resulting in an impossibility to predict if and in what fashion a molecule will self-assemble on a chosen surface. Nevertheless, one can drastically increase their chances to successfully find ordered structures by making an educated guess. In the following paragraphs various parameters and their influence onto the layer formation will be discussed.

### Geometrical Properties: Size of Atoms and Symmetry

The crystal structure of both silver and copper is face-centered cubic. The lattice constant of silver is 4.09 Å and the one of copper 3.61 Å [79]. From this it is easy to deduce the geometry and distance between two surface atoms. Thus, the Ag(100) features a surface with atoms arranged in square configuration and a distance of 2.89 Å. Both the Ag(111) and Cu(111) feature hexagonal surfaces with nearest neighbor distances of 2.89 Å and 2.55 Å respectively. The leg spacing of  $\approx 12\text{Å}$  thus spans the length of about 4 to 5 atoms. Considering that the molecules may adopt an arbitrary angle relative to the main substrate direction the molecule should always easily find a way to adsorb in the energetically preferred way, no matter if the di(tert-butyl)phenyl legs prefer top sites, hollow sites or bridge sites. In addition, the possibility of deforming the molecule as discussed in section 3.2 further increases the adoptability of the molecules to dif-

ferent atom-atom distances of the substrate. Such deformations should not incur large energy penalties if the deformations are only small compared to the relaxed configuration.

The symmetry of the arrangement of the surface atoms on the other hand seems to play an obvious role. Ag(100) with the square arrangement of the surface atoms has a fourfold symmetry. Ag(111) and Cu(111) display the threefold symmetry of the hexagonal surface. While DMP molecules on Ag(100) adopt an almost square arrangement they feature a distinctly hexagonal pattern on Ag(111). The assembly on Cu(111) reflects an intermediate case. The hole phase displays an ordering close to the hexagonal symmetry and the close-packed phase features considerably more complexity by alternating rows of molecules with different rotational orientation. The close-packed phase on Ag(111) seems to contradict this observation at first glance. However, one needs to remember that this arrangement only emerged after annealing and it features considerably greater distances than the one on Ag(100) resulting in an areal density of only half of that of the Ag(100) arrangement. Thus it can be concluded that the symmetry of the substrate atoms is one of the major geometrical influences on the resulting ordering.

### Physisorption

A. Zangwill defines physisorption (or physical adsorption) as being characterized "by the lack of a true chemical bond between adsorbate and substrate" [80]. The IUPAC (International Union of Pure and Applied Chemistry) further notes that the border between chemisorption and physisorption can be fuzzy and that intermediate cases exist [81]. The DMP molecules adsorbed on metal surfaces are only weakly bound, as can be evidenced from the existence of the gas phases described earlier. Thus, the process observed here rather resembles physisorption than chemisorption. Nevertheless it will be argued in the following that ionic interactions or interactions involving  $\pi$  orbitals may be present in addition to the ever present vdW interactions.

VdW interactions arise from dynamic dipole-dipole interactions and are very weak, smaller than 50 meV [82]. VdW forces will be present both between molecules and surface as well as between adjacent molecules (see section 3.3). However, differences between vdW interactions of the same molecule on the various substrates do not seem likely to be of any great importance since the forces are expected to be of a similar order of magnitude in all cases. Even though the porphyrin macrocycles can act as electron donors it seems unlikely that a significant charge transfer will take place between the porphyrin and the metal due to the di(tert-butyl)phenyl substituents which raise the porphyrin core from the surface. This assumption is supported by experiments conducted on Ni(II)



octaethylporphyrin which showed that no charge transfer between metal surface and porphyrin core even though the spacer legs were considerably smaller [83].

In section 3.3 the possibility of molecule-molecule interaction through weak H-bonds between the cyano moiety and respective H atoms of neighboring molecules was discussed. Additionally, measurements conducted by Stevens et al. have shown that cyano groups tend to adsorb on metals with the C-N bond parallel to the substrate surface [84]. They suggested that an interaction involving  $\pi$ -donation occurred. For example, acetonitrile adsorbed on Ag(100) with a binding energy of 0.4 eV. Even though the cyanophenyl moieties can rotate around the  $\sigma$ -bond to the porphyrin, the length of the bonds can not change considerably. Assuming that this interaction favors a certain metal site (e.g. on top of a metal atom) the problem of the metal atoms coinciding with the C-N bond may be of great importance which would also explain the dependence upon the distance between surface atoms. Furthermore, the interaction between the cyano groups and different metals is of different strength, introducing a dependency on the kind of metal.

### Surface states

One possible type of adsorbate-surface interaction has not been discussed in the previous section on purpose. This interaction has been made visible with STM measurements as opposed to the 'ordinary' interactions described above. It has been shown that disturbances on surfaces such as defects or adsorbed molecules lead to oscillations in the surface charge density [85]. This effect is explained by interference between the electron wave travelling towards the adsorbed molecule and the backscattered wave which leads to a standing wave with a wavelength of half of the Fermi wavelength. The resulting oscillation in the LDOS can be observed in STM experiments as demonstrated for example in the famous measurement where a standing wave has been created inside a *quantum coral* [86]. Furthermore, experiments have shown that these surface oscillations can lead to long range interactions between atoms or molecules adsorbed on surfaces [85, 87–92]. For Ag(111), the periodicity of such standing waves around a perfectly scattering adsorbate would be 3.8 nm. For real adsorbates, e.g. such as Ce atoms on Ag(111), this value reduces to 3.2 nm because of the imperfect scattering properties of the adsorbed metal atom [89]. Even though this distance is far greater than the observed distance between neighboring molecules in the assemblies it nicely fits with the pore-pore distance measured in the porous network. Furthermore, the electronic interaction between molecules and surface is not very strong, as discussed above. Thus, it does not seem very likely that surface oscillations play a major role in forming the porous structure. However, it seems quite probable that this effect is influencing the interaction between individual fullerenes adsorbed into the network, as will be argued later.

## 4.5 C<sub>60</sub> - DMP Assemblies on Ag(100)

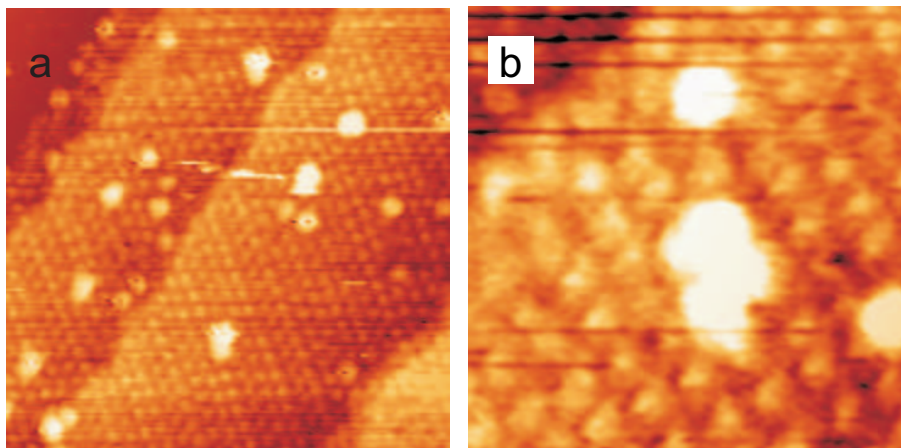


Figure 4.8: STM images of C<sub>60</sub> on DMP on Ag(100). a) Overview STM image (scan range:  $40 \times 40 \text{ nm}^2$ ,  $V_{bias} = 3.01 \text{ V}$ ,  $I_t = 10 \text{ pA}$ ,  $T = 298 \text{ K}$ ) revealing the presence of fullerene aggregates and disordered individual C<sub>60</sub> molecules. b) Detailed STM image (scan range:  $13 \times 13 \text{ nm}^2$ ,  $V_{bias} = 3.01 \text{ V}$ ,  $I_t = 10 \text{ pA}$ ,  $T = 298 \text{ K}$ ) showing a fullerene cluster adsorbed on top of a well ordered porphyrin layer.

C<sub>60</sub> molecules have been sublimed onto a preadsorbed ordered layer of DMP molecules on Ag(100). STM images of the resulting system can be seen in figure 4.8. Between monoatomic steps of the surface one can recognize the monolayer of DMP molecules occupying the terraces in the middle of figure 4.8a. The deposited C<sub>60</sub> molecules show up on the scans as relatively large protrusions of various shapes. The apparent height of the protrusions was measured to be about 6 to 8 Å. This indicates that the fullerenes do not stack vertically. Unfortunately, single C<sub>60</sub> molecules could not be resolved in these images. However, judging from the lateral dimensions of the protrusions the clusters consist of a few C<sub>60</sub> molecules. Imaging these samples is very hard due to permanent tip changes. This indicates that the fullerene molecules are only loosely bound to the DMP layer and either mobile on the surface or easily influenced by the STM tip, even at scanning conditions. This combination of porphyrin molecules and metal substrate does not seem to be appropriate for supporting structures capable of inducing ordered fullerene assemblies.

## 4.6 C<sub>60</sub> - DMP Assemblies on Ag(111)

Upon subsequent sublimation of C<sub>60</sub>, single fullerene molecules adsorbed into the pores introduced in section 4.3. Similar to the observations reported in section 3.4, no molecules adsorbed on top of the porphyrin units. Instead, the fullerenes



seemed to prefer to adsorb near the cyanophenyl moieties as can be seen in figure 4.9. At increased guest molecule coverage (figure 4.9a) notable deviations from the expected statistical distribution of the fullerenes occurred. The C<sub>60</sub> started condensing into areas of high guest molecule coverage right next to areas without guest molecules. Furthermore, one can observe an exceptionally large number of fullerene chains and island. This behavior is indicative of a system with forces interaction between the guest molecules. Similar behavior has been reported for nanoporous networks before [93].

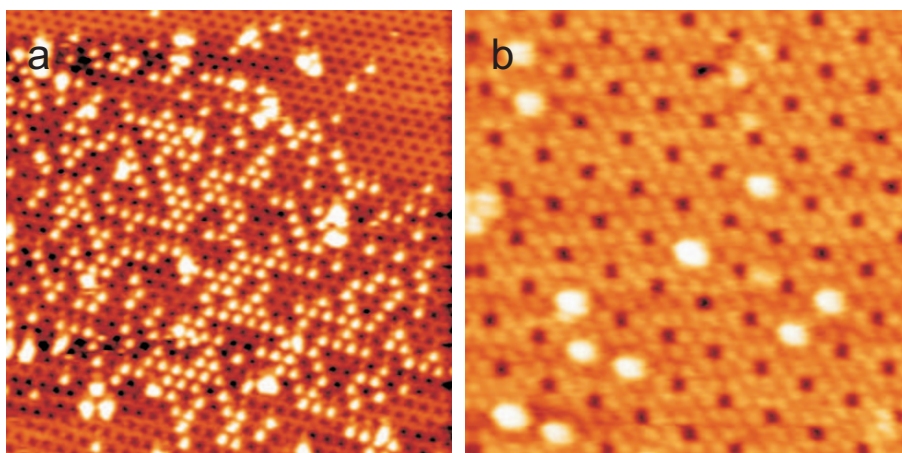


Figure 4.9: STM images of C<sub>60</sub> on porous DMP assembly on Ag(111). a) Overview STM image (scan range:  $100 \times 100 \text{ nm}^2$ ,  $V_{bias} = 3.00 \text{ V}$ ,  $I_t = 9 \text{ pA}$ ,  $T = 298 \text{ K}$ ). The C<sub>60</sub> display a distinctly non-stochastic distribution, forming 1D lines and 2D clusters. b) Detailed STM image (scan range:  $30 \times 30 \text{ nm}^2$ ,  $V_{bias} = 2.90 \text{ V}$ ,  $I_t = 12 \text{ pA}$ ,  $T = 298 \text{ K}$ ) clearly resolving the underlying porous DMP assembly and showing that the fullerenes adsorb into the pores.

Time-lapse STM images (figure 5.3, next chapter) revealed a rather high probability for lateral displacement of the C<sub>60</sub> molecules at RT. At low guest molecule coverage ( $\approx 0.01 \text{ ML C}_{60}$ ) the displacement occurred with a rate of approximately  $10^{-3} \text{ s}^{-1}$ . In order to minimize the influence of the tip on the hopping process all STM data were acquired with a high tunneling gap resistance of more than  $100 \text{ G}\Omega$ .

Interestingly, thermal annealing to 450K of mixed DMP-C<sub>60</sub> samples led not only to the expected phase separation into pure DMP and pure C<sub>60</sub> islands (e.g. section 3.5) but also to the formation of the phase shown in figure 4.11. This extraordinary DMP-C<sub>60</sub> phase features fullerenes arranged in ordered pairs. The C<sub>60</sub>-C<sub>60</sub> distance of such a pair is 2.3 nm while the pair-pair distance is  $X_{pair} = 6.0 \text{ nm}$  and  $Y_{pair} = 7.3 \text{ nm}$ . Domains of up to  $50 \times 100 \text{ nm}^2$  have been found. Pure DMP islands coexist right next to the paired phase as well as mobile molecules

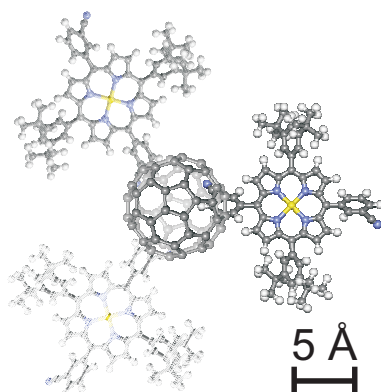


Figure 4.10: Proposed model of a  $C_{60}$  adsorbed on the porous DMP assembly on Ag(111) depicting the respective sizes. In the STM images (figure 4.9) the lateral diameter of the  $C_{60}$  appear larger due to tip corrugation.

(streaky areas). No diffusion of  $C_{60}$  adsorbed in the pair phase has been observed at RT.

Both assemblies presented in this section feature long range ordering of the  $C_{60}$  molecules over distances of 3.3 nm (porous phase) up to 7.3 nm. This excludes any significant contribution of direct fullerene-fullerene forces (e.g. vdW forces). Instead, interactions mediated by the substrate and/or the molecular porphyrin layer must be considered. This will be discussed in detail in section 5.6 considering the case of the porous network. However, analogous considerations are also valid for the pair phase.

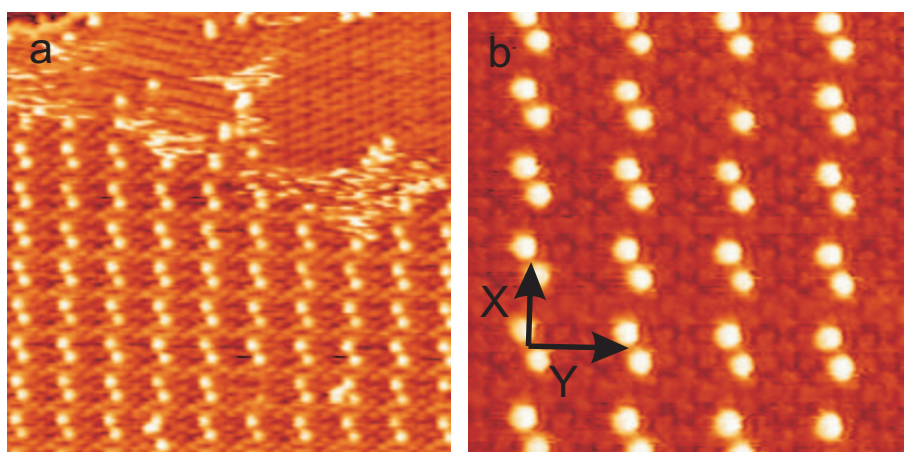


Figure 4.11: STM images of  $C_{60}$ -pair phase on DMP on Ag(111). a) Overview STM image (scan range:  $68 \times 68 \text{ nm}^2$ ,  $V_{bias} = 1.97 \text{ V}$ ,  $I_t = 64 \text{ pA}$ ,  $T = 298 \text{ K}$ ). b) Detailed STM image (scan range:  $30 \times 30 \text{ nm}^2$ ,  $V_{bias} = 2.67 \text{ V}$ ,  $I_t = 16 \text{ pA}$ ,  $T = 298 \text{ K}$ ). This interesting arrangement appeared after thermal annealing of a Ag(111) substrate covered with DMP and  $C_{60}$  as shown for example in figure 4.9.



## Chapter 5

# Adsorption and Dynamics of Hosted Fullerenes

It has been noted in section 4.6 that the  $C_{60}$  molecules show a disposition for lateral displacement due to thermal activation at 298 K. This chapter will analyze these movements in detail. In order to investigate this, it has been found meaningful to vary not only the guest molecule coverage but moreover to exchange the molecules hosted in the pores. For this reason,  $C_{70}$  molecules were evaporated onto the same hexagonal porphyrin network for comparison.

### 5.1 Adsorption of $C_{60}$ and $C_{70}$ in the Host-Network

At first glance, STM images of  $C_{70}$  and  $C_{60}$  on the porous porphyrin lattice seem very similar (figure 5.3). Both guest molecules adsorb concentrically into the pores of the underlying network and appear as bright protrusions with an indistinguishable lateral diameter of  $1.7 \pm 0.3$  nm (full-width at half maximum), as exemplarily shown by the line cuts in figure 5.1. Note that due to the finite size of the STM tip, the lateral dimensions of single molecules are broadened by the tip-surface convolution. In contrast to the work of Katsonis et al., who found  $C_{70}$  molecules with an elliptical shape at a Au(111) surface [94], the fullerenes on the porphyrin network always appear with spherical symmetry. As well, no submolecular structure of the  $C_{70}$  spheres could be observed, as opposed to the intermixed  $C_{60}$  /  $C_{70}$  monolayer on Cu(111) reported by Wang et al. [31]. This difference may be caused by the relatively weak adsorption energy of the fullerenes in the present porphyrin framework compared to the stronger metal-fullerene interaction in the above-mentioned reports which forces the  $C_{70}$  molecules to adsorb steadily with the long side parallel to the surface. This indicates that the fullerenes in the pores of the supramolecular assembly of DMP are able to vibrate and rotate at 298 K which is confirmed by their averaged round appearance on the time scale of STM measurements. However, it is expected that  $C_{60}$  and  $C_{70}$  can be discriminated by

their different apparent heights in STM [31, 94]. For a meaningful analysis, the apparent height measurements (figure 5.1) need to be normalized before they can be compared, in order to account for different STM tip geometries. It has been shown [95, 96] that this can be achieved by normalizing the height histogram of two different measurements with a characteristic peak, corresponding to a common substructure in the two STM images. In the present study the apparent height of the pure porphyrin network provides a suitable point of reference since it very likely shows a constant corrugation, independent of the presence of guest molecules. Figure 5.2 shows histograms of apparent heights of three representative STM images.

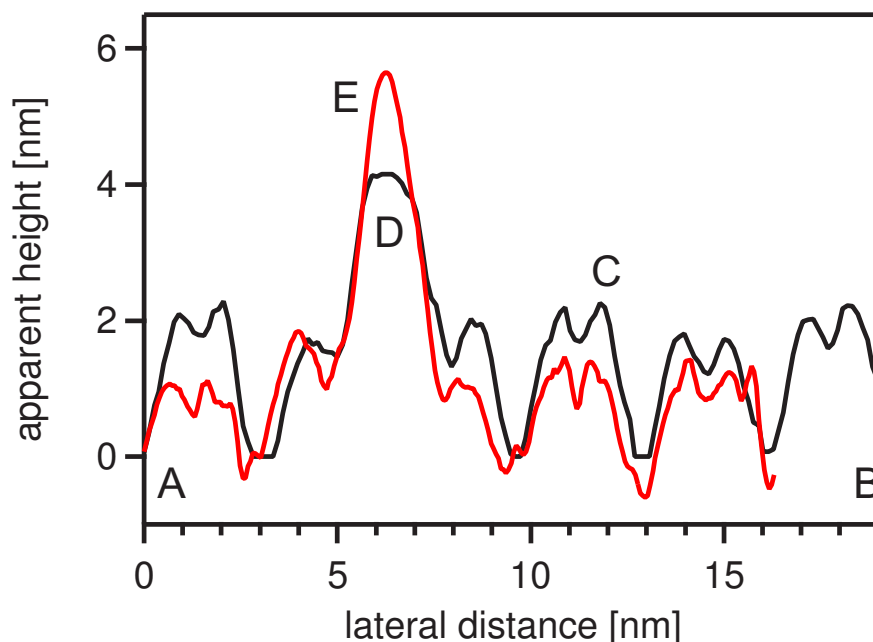


Figure 5.1: Line sections of the porphyrin network (label C) with  $C_{60}$  (black) and  $C_{70}$  (red) from measured data along the black lines from A to B as indicated in figure 5.3.

The curves have been normalized by adjusting the position, the width, and the height of the dominant peak (label C), representing the porphyrin layer. In the detailed view (inset of figure 5.2) one can clearly see that the normalized curves of  $C_{60}$  (blue) and  $C_{70}$  (red) feature distinctly different cut-off positions, as indicated by labels D and E, respectively. These characteristic features which are completely absent when no guest molecules are present (black), reflect the maximum height in each STM image and are caused by the fullerene guests. Applying this method, the ratio of the measured height of  $C_{70}$  [ $h_a(C_{70})$ ] to that of  $C_{60}$  [ $h_a(C_{60})$ ] was calculated to  $h_a(C_{70})/h_a(C_{60}) = 1.5 \pm 0.1$ . This result was found to be in-

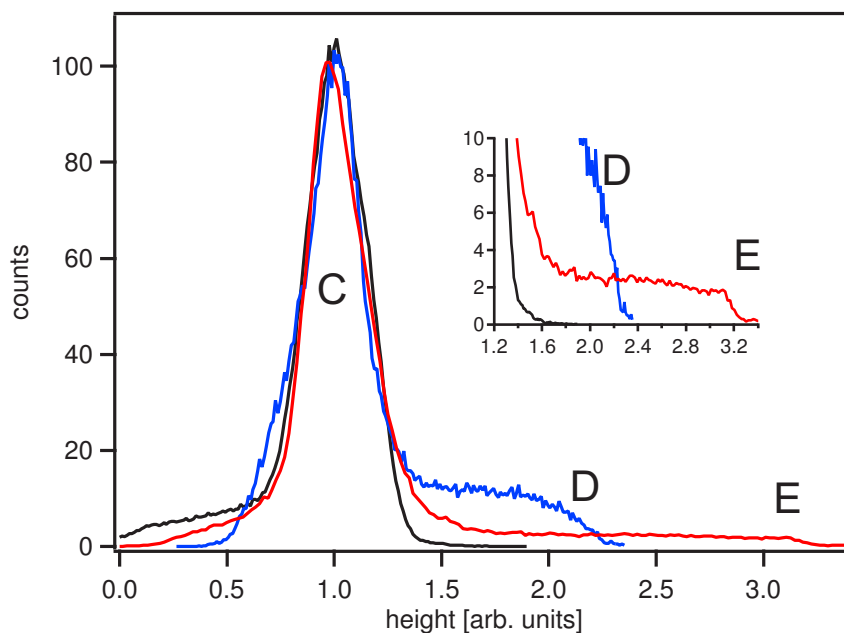


Figure 5.2: Normalized histograms of the distribution of apparent heights for a clean porphyrin network (black), a porphyrin network with  $C_{60}$  (blue) and one with  $C_{70}$  (red). The inset shows the cut off positions of  $C_{60}$  and  $C_{70}$  (labels D, E) in detail.

dependent of the quality of the STM images caused by different tip geometries and the guest molecule coverage. Scan parameters such as bias voltage, scan size, or scan speed did not affect the height ratio either. The value of  $\approx 1.5$  for the measured height ratio deviates significantly from the maximum ratio of  $\approx 1.13$  which is obtained by pure geometrical consideration of the vdW-diameter of the two fullerenes [ $d(C_{60}) \approx 10.6 \text{ \AA}$  [97, 98];  $d_{max}(C_{70}) \approx 12.0 \text{ \AA}$  [21, 22] (see section 1.2.2)]. A similar observation has been reported for co-deposited  $C_{60}$  and  $C_{70}$  monolayer on Au(111) where the height ratio  $h_a(C_{70})/h_a(C_{60})$  was determined as  $1.4 \pm 0.2$  from an analysis of STM cross-sections [94]. Since topographic differences can be excluded in that case where both fullerenes were in direct contact with the metal substrate, the increased height ratio can be purely attributed to different electronic metal-fullerene coupling. For the fullerenes adsorbed within the porphyrin-based pores, the situation is even more complicated. On the one hand, the different electronic properties of  $C_{70}$  compared to those of  $C_{60}$  (e.g. electron affinity, ionization potential, or HOMO-LUMO gap [17]) are expected to result in unequal host-guest interactions. On the other hand, the oblong shape of  $C_{70}$  compared to the spherical shape of  $C_{60}$  likely demands a different adsorption geometry in the pores, either by standing upright, lying on the long side (thus not fitting as far down the pore), or some (dynamic) variation of those two. Overall, the measured height ratio is indicative of a dissimilar interaction with the pores

and therefore the host-guest interaction energies for the two fullerene molecules are expected to be different.

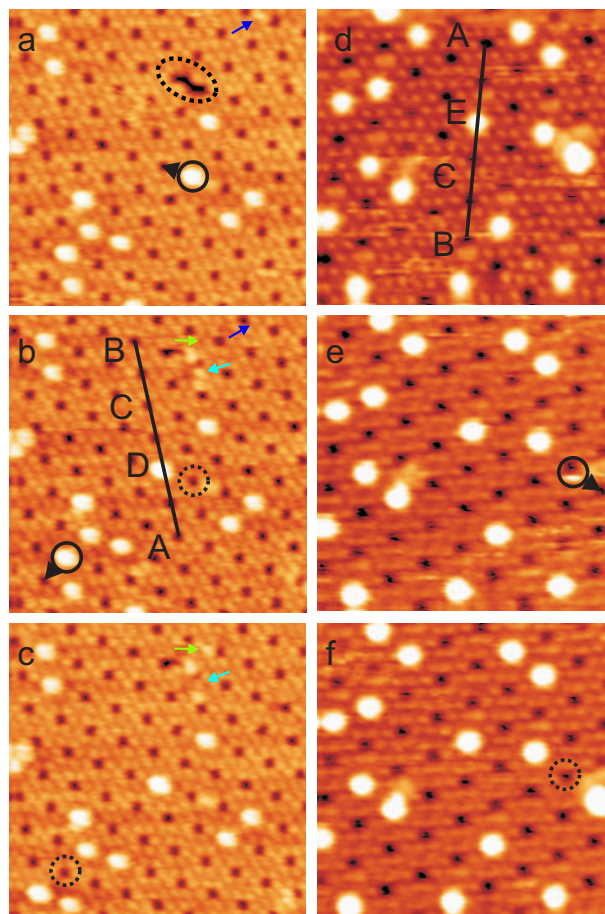


Figure 5.3: a) - c) Series of consecutive STM images of  $C_{60}$  (label D) molecules on the porous porphyrin network (scan range:  $30 \times 30 \text{ nm}^2$ ,  $V_{bias} = 2.90 \text{ V}$ ,  $I_t = 12 \text{ pA}$ ,  $T = 298 \text{ K}$ ). The time lapse between two measurements is 62 s. d) - f) Series of consecutive STM images of  $C_{70}$  (label E) molecules on the porous porphyrin network (scan range:  $25 \times 25 \text{ nm}^2$ ,  $V_{bias} = 2.00 \text{ V}$ ,  $I_t = 12 \text{ pA}$ ,  $T = 298 \text{ K}$ ). The time lapse between two measurements is 89 s. Closed circles indicate molecules which moved between subsequent pictures, dashed circles indicate former positions of molecules.

## 5.2 Mobility of Single Fullerene Molecules

In order to investigate the mobility of the guest molecules, time-lapse imaging experiments were performed as shown in figure 5.3a-f. In both series, individual fullerenes ( $C_{60}$  and  $C_{70}$ ) were found to move from one pore to a neighboring one by thermal activation at 298 K. On the timescale of one STM measurement



(from one to a few minutes) only some molecules moved while most stayed at their adsorption site. This singles out STM as an adequate technique to examine the dynamics of these fluctuating supramolecular structures. In order to minimize the potential influence of the scanning on the hopping process, all images were recorded using a large tunneling-gap resistance of more than 100 G $\Omega$ . By analyzing the positions of a large number of molecules over several consecutive STM images, one can determine the respective displacements and their relative occurrence in dependence of the elapsed time. Practically, the position of 200–1000 fullerene molecules (number depending on the available STM data) were observed and analyzed in displacement histograms as exemplarily shown for C<sub>60</sub> in figure 5.4.

The peaks in the histogram, which are centered around the discrete distances of a hexagonal porous lattice as depicted in figure 5.4a, clearly show that the guest molecules move by means of a hopping process from pore to pore. This finding is consequent to the fact that the guest molecules are restricted to occupy only pore sites. Thereby, a big part of the observed guest molecules did not perform a jump (80% – 90%). The great majority of the molecules that did jump, moved to a nearest neighbor (NN) position (10%, red arrow). Some moved to the  $\sqrt{3}$ NN pore (1%, green arrow) and another 1% moved to the 2NN pore (blue arrow). However, we will argue later that most of the long jumps (>NN-distance) may be caused by two consecutive single jumps. In order to obtain information about the hopping rates, one has to determine the probability  $P_{(0)}(\tau)$  that a molecule does not move in the time interval  $\tau$  it takes to record the STM image. Using the relation  $P_{(0)}(\tau) = \exp(-h\tau)$ , which results from Poisson statistics, allows thus to calculate the hopping rate  $h$  of the examined system [99–102]. The number of observed molecules and the time  $\tau$  then determine the statistical certainty of the hopping rate  $h$ . Because such a simplified approach does not account for multiple jumps, the resulting  $h$  will be systematically underestimated [102].

Using this procedure, a pronounced difference in the hopping rates of C<sub>60</sub> [ $h(\Theta = 0.06) \approx 1 \times 10^{-3} \text{ s}^{-1}$ ] and C<sub>70</sub> [ $h(\Theta = 0.01) \approx 9 \times 10^2 \text{ s}^{-1}$ ] has been found at the lowest measured guest molecule coverage. Since under such dilute conditions the lateral inter-fullerene interactions are minimal, these values approximately reflect the different jump barriers  $E_a(\Theta \approx 0)$  for a single isolated guest molecule. A quantitative estimation of the diffusion barrier close to zero coverage can be obtained by using the relation

$$h(\Theta \approx 0) = \nu_0 \exp\left(-\frac{E_a(\Theta \approx 0)}{kT}\right) \quad (5.1)$$

where  $\nu_0$  is the attempt frequency [39, 80, 100]. Assuming a standard value of  $\nu_0 = 10^{13} \text{ s}^{-1}$ ,  $E_a(\Theta \approx 0)$  was calculated to be  $0.95 \pm 0.18 \text{ eV}$  and  $0.82 \pm$

0.18 eV for  $C_{60}$  and  $C_{70}$ , respectively. The relatively large error is due to the uncertainty in the attempt frequency for which a lower limit of  $10^{10} \text{ s}^{-1}$  and an upper limit of  $10^{16} \text{ s}^{-1}$  was assumed [100]. Expecting the attempt frequency for both systems to be equal, the difference between the diffusions barriers of the two fullerenes can be calculated to be approximately  $0.13 \pm 0.01 \text{ eV}$ . These findings reflect the above discussed differences in host-guest interaction (manifested in the apparent heights) of the two types of fullerenes. Compared to  $C_{60}$ ,  $C_{70}$  is obviously less effectively trapped within the porous framework and consequently a lower activation energy for diffusion is found.

### 5.3 Jump Lengths

Since the determination of the hopping rates and the jump distances have been performed with a statistical ensemble of indistinguishable molecules, one can calculate the expected jump length  $\lambda$  with the help of the hopping rate  $h$  and the mean squared displacement  $\langle(\Delta x)^2\rangle$  using relation 5.2: [102]

$$\langle(\Delta x)^2\rangle = \lambda^2 h \tau \quad (5.2)$$

Analysis of our data yielded values of  $\lambda = 4.5 \pm 0.3 \text{ nm}$  for  $C_{60}$  and  $\lambda = 4.2 \pm 0.2 \text{ nm}$  for  $C_{70}$ . These values correspond to  $1.4 \pm 0.1$  and  $1.3 \pm 0.1$  times the pore-pore distance of  $3.3 \text{ nm}$ , respectively. The jump length turned out to be independent of the fullerene coverage to the extent to which could be determined in these experiments. These results clearly show that the present system is mainly ruled by single jumps with a few contributions from long-jumps. In contrast to the distinct differences between the hopping rates of  $C_{60}$  and  $C_{70}$ , their jump lengths are not distinguishable.

### 5.4 Coverage Dependent Hopping Rates

When increasing the fullerene coverage, the formation of short chains and islands of guest molecules can be observed as shown in figure 4.9. Interestingly, for  $C_{70}$  this behavior was already found at considerably low coverage ( $\Theta \approx 0.1$ ) whereas for  $C_{60}$  it has only been observed at higher values ( $\Theta > 0.5$ ). These findings clearly indicate a distinct interaction between the guest molecules which likely influences their mobility. Therefore, a systematic investigation of the hopping rates as a function of the fullerene coverage has been performed. Figures 5.5a and b show the hopping rates of the  $C_{60}$ -DMP and  $C_{70}$ -DMP assemblies as a function of the fullerene coverage.

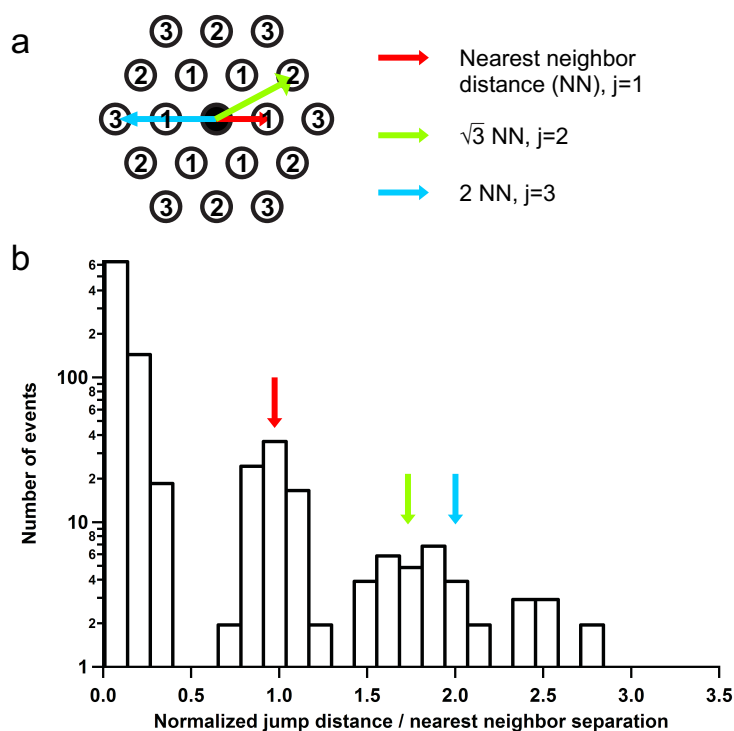


Figure 5.4: a) Schematic representation of the 2D porous hexagonal network. The numbers indicate the index  $j$  of the distance between the center and the respective neighboring site. The colored arrows indicate the nearest ( $NN$ , red), next nearest ( $\sqrt{3}NN$ , green), and second nearest neighbor ( $2NN$ , blue) distances. b) Example of a histogram of jump distances of  $C_{60}$  on the porous porphyrin network. The position of 939 guest molecules in an STM movie (scan range:  $100 \times 100 \text{ nm}^2$ , scan speed: 144 s per frame, 14 frames) was analyzed over a time period of totally 33 min. Note the distinct peaks at 1, 1.73 and 2 nearest neighbor distances. The spreading of the peaks is caused by the inhomogeneous drift during scanning which alters the imaged pore-pore distances.

One can clearly see that the two curves follow distinctly different trends which deviate considerably from a simple linear relation described below. The hopping rate of  $C_{60}$  increases between a coverage of zero and 0.3 followed by a strong decrease of the rate at higher values. In contrast, the hopping rate of  $C_{70}$  starts decreasing strongly right away and rapidly reaches a value which is about two orders of magnitude lower. It should additionally be noted that annealing of the samples to 400 K with subsequent cooling down to 298 K did not significantly affect the guest molecule distributions or hopping rates. These findings clearly indicate that the investigated host guest-systems are in thermal equilibrium. A semi-quantitative interpretation of the coverage dependence can be done within the lattice gas or Bethe-Peierls approximation [103]. Thereby, adparticles (fullerenes in this case) are restricted to occupy only predefined sites (porphyrin pores here) on a rigid host lattice and each of these adsorption sites is capable of

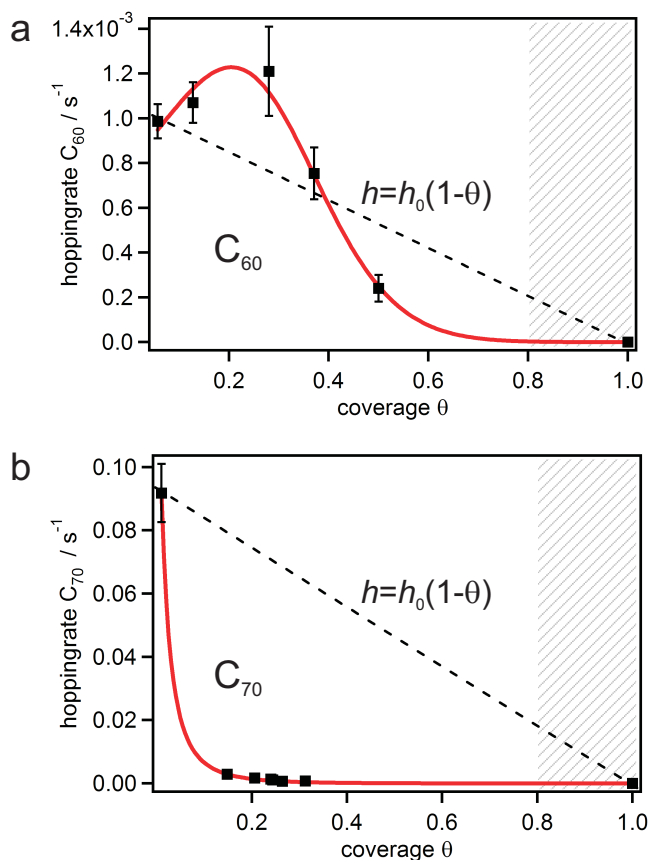


Figure 5.5: Coverage dependent hopping rate of C<sub>60</sub>. The square markers indicate the data points as determined from the analysis of the STM data, with the uncertainty indicated by the error bars. The red line represents the best fit to the quasi-chemical approach as described in the main text. The dashed line shows the linear dependence of the hopping rate as predicted by the lattice gas model with pure site blocking. The hatched area indicates coverage where the networks break down. b) Coverage dependent hopping rate of the C<sub>70</sub> molecules.

hosting exactly one guest particle. Driven by thermal activation, particles are allowed to perform random jumps to neighboring positions of the lattice only if the target site is empty. This so-called site-blocking mechanism prevents the adsorption sites from double occupancy. The coverage dependence of the hopping rate within this approximation accordingly leads to  $h(\Theta) = h_0(1 - \Theta)$ , when further neglecting any inter-particle interactions ( $h_0$  denotes the rate of a single particle in an infinitely diluted environment). The straight dotted line in figures 5.5a and b indicates this simplest model for the coverage dependence of the hopping rate. Obviously, the present systems do behave somewhat more complicated since the formation of guest molecule chains and islands can be observed upon increasing the fullerene coverage (figure 4.9). Such systems of interacting particles in a lattice gas have been addressed within the quasi chemical approach [103–105]. In

		C <sub>60</sub>	C <sub>70</sub>
diffusion barrier	$E_a$ [eV]	$0.95 \pm 0.18$	$0.82 \pm 0.18$
QCA parameters	$h_0$ [s <sup>-1</sup> ]	$7.9 \pm 0.7 \times 10^{-4}$	$1.3 \pm 0.2 \times 10^{-1}$
	$E_0$ [meV]	$+31 \pm 10$	$-58 \pm 20$
	$E'$ [meV]	$-71 \pm 18$	$\approx 0$
Jump lenght	$\lambda$ [nm]	$4.5 \pm 0.3$	$4.2 \pm 0.2$

Table 5.1: Overview of the estimated energies present in the porphyrin-fullerene host-guest systems and the parameters for the quasi-chemical approach (QCA). The QCA parameters are fitted values according to equations 5.3-5.7. The diffusion barriers and jump lengths were calculated using equations 5.1 and 5.2, respectively.

this approximation, the coverage-dependent hopping rate  $h(\Theta)$  can be analytically expressed as

$$h(\Theta) = h_0 \frac{(1 + \varepsilon)^{z-1}}{(1 + \frac{\varepsilon}{f})^z} \quad (5.3)$$

with

$$\varepsilon = \frac{(\beta - 1 + 2\Theta)f}{2(1 - \Theta)} \quad (5.4)$$

$$\beta = \sqrt{1 - 4\Theta(1 - \Theta)(1 - \frac{1}{f})} \quad (5.5)$$

$$f = \exp\left(\frac{E_{int}}{kT}\right) \quad (5.6)$$

where  $z$  is the coordination number which equals 6 in the case of a hexagonal lattice. Furthermore, adparticles on the rigid lattice are supposed to interact with each other only through nearest neighbor forces, characterized by the interaction energy  $E_{int}$  (equation 5.6). Each additional nearest neighbor particle increases/reduces the binding energy of an adparticle by  $E_{int}$  and therefore affects its jump probability. The parameter  $f$  in equation 5.6 indicates the nature of the interaction: either attracting for  $f < 1$  (which reduces the hopping rate) or repelling for  $f > 1$  (resulting in an increase of the ad-particle mobility). However, this approach with constant interaction energy  $E_{int}$  does not necessarily match the behavior of real systems. In zeolites for example, Krishna et al. [104] applied a linearly coverage dependent interaction energy which accounts for the ad-particle-induced modification of the lattice sites or cooperative guest effects:

$$E_{int}(\Theta) = E_0 + E'\Theta \quad (5.7)$$

Here,  $E_0$  is the interaction energy at zero coverage and  $E'$  is the slope of  $E_{int}(\Theta)$  as a function of coverage. Consequently, the experimentally derived hopping rates of the fullerene guest molecules on the porous porphyrin network have been fitted with equations 5.3 and 5.7. The data point  $h(\Theta = 1) = 0$  which always exists in a lattice gas has been enclosed in the data set in order to improve the fit quality. Nevertheless, it should be noted that around a coverage  $\Theta > 0.8$ , the complete porphyrin network collapses irreversibly for both fullerenes structures. The solid lines in figure 5.5a and b represent the fits to the experimental data, whereby the values listed in table 1 have been obtained for the fitting parameters  $h_0$ ,  $E_0$  and  $E'$ . Figure 5.5c shows the trend of the interaction energy  $E_{int}$  explicitly as a function of coverage as calculated by equation 5.7.

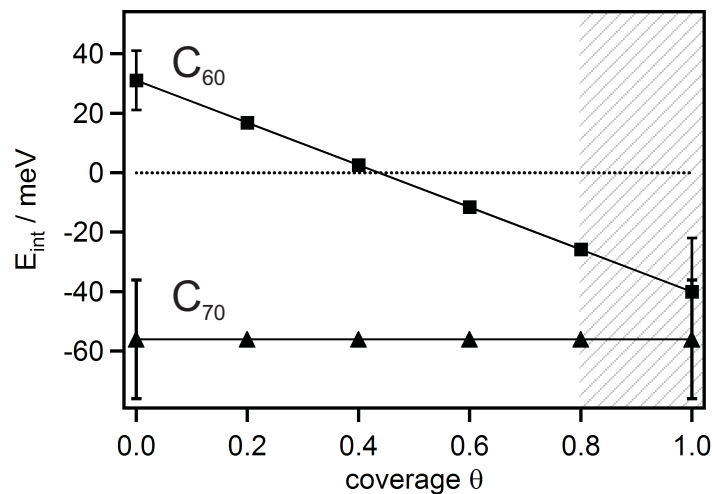


Figure 5.6: Interaction energies of the  $C_{60}$  and  $C_{70}$  as a function of coverage according to equation 5.7 using the values given in Table 5.1.

In order to compare the actual hopping rates with existing diffusion data, the self-diffusivity of the fullerenes may be estimated by using the relation [104–106]

$$D_{self} = \frac{1}{4}h(\Theta)\lambda^2 \quad (5.8)$$

For a given lattice, like in this case, this procedure is basically a multiplication with a constant and therefore the qualitative trend of the hopping rates and self-diffusivity can directly be compared. According to the quasi-chemical approximation, the pronounced decrease in the hopping rate of  $C_{70}$  is caused by the presence of a distinct attractive interaction between the nearest neighbor molecules. This can be deduced from the negative value of  $E_{int} = -58 \pm 20$  meV (figure 5.5c). Within the calculated error, the interaction energy has been found to be constant (i.e.  $E' \approx 0$ ) over the whole fullerene coverage range. It is worth to note that the value of  $E_{int}$  is comparable with the one of Xe atoms on

a Pt(111) surface at  $T = 80$  K, where a coverage independent nearest neighbor interaction energy  $E_{int} \approx -10$  meV between the diffusing rare gas atoms has been found using the same lattice gas model [107]. In contrast, the situation with  $C_{60}$  is remarkably different. At low coverage, a repulsive nearest neighbor interaction ( $E_{int} > 0$ ) is effective.  $E_{int}$  then decreases with increasing coverage and becomes attractive ( $E_{int} < 0$ ) above  $\Theta \approx 0.45$  as shown in figure 5.5c. Unlike in the case of  $C_{70}$ , it is not possible to fit the experimental data with a constant interaction parameter. Similar trends have also been reported in theoretical calculations of self-diffusivity in zeolites: as shown by Krishna et al. [104],  $CH_4$ , Ar, or Ne in ITE-type zeolites at 298 K can be interpreted within the quasi-chemical approach using a linearly decreasing interaction energy (equation 5.7). These systems change their character from repulsive at low coverage to attractive in the high loading regime, analogously to the system described here.

## 5.5 Pair Distribution

However, one should keep in mind that so far all results were derived from a semi-empirical lattice gas model which is based on several severe simplifications. It is therefore worth to double check the results obtained by this dynamic analysis with another independent method. This can be performed by analyzing the 2D pair distribution of the guest molecules on the porous network from static STM images. In contrast to the dynamic examination in section 5.4, the pair distribution function reflects deviations of the observed guest molecule arrangement compared to a random particle distribution. Trost et al. explicitly derived the pair distribution function  $g(j)$  for particles adsorbed on discrete lattice sites as

$$g(j) = (N\Theta)^{-1} \sum_{i=1}^N \frac{n_i(j)}{m(j)} \quad (5.9)$$

where  $n_i(j)$  is the number of particles around a particle  $i$  occupying the  $j$ th nearest neighbor site [108]. The denominator  $m(j)$  accounts for the totally available adsorption positions at the  $j$ th nearest neighbor distance (figure 5.4a). Normalization of the distribution is achieved by dividing with the coverage. Practically, deviations from  $g = 1$  indicate a divergence from the stochastic distribution and thus imply the presence of an attractive or repulsive inter-particle force for  $g > 1$  or  $g < 1$  respectively. The pair distribution functions  $g(j)$  for  $C_{60}$  (squares) and  $C_{70}$  (triangles), as shown in figure 5.7, have been derived from the positional analysis of several hundred fullerene molecules in different uniform STM images in the low coverage regime.

As can be seen from figure 5.7, the pair distribution functions of the two fullerenes clearly exhibit different trends. While for  $C_{70}$   $g(1) = 1.5$  indicates an attractive interaction,  $g(1) = 0.7$  for  $C_{60}$  shows the presence of repulsive forces

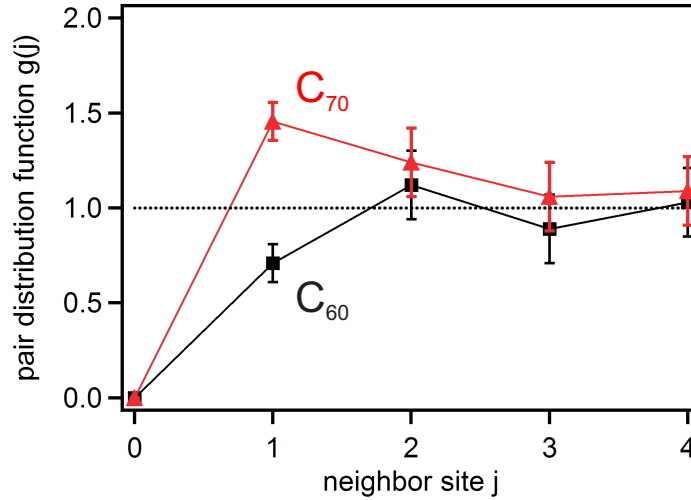


Figure 5.7: Pair distribution  $g(j)$  as a function of neighbor site  $j$  for  $C_{60}$  (squares) and  $C_{70}$  (triangles) according to equation 5.9 as obtained from several STM images ( $\Theta = 0.1$  for  $C_{60}$  and  $\Theta = 0.2$  for  $C_{70}$ ). A definition for  $j$  is given in the scheme in figure 5.4a. Especially note the pronounced difference between the two fullerenes at  $j = 1$  which qualitatively reflects the result obtained within the quasi-chemical approach.

between nearest neighbor fullerenes. In the case of  $C_{70}$ , the distribution function stays slightly above unity at  $j = 2$  and then runs toward the average occupation probability for  $j > 2$  (for  $C_{60}$   $g(j) \approx 1$  already for  $j > 1$ ). As a result, both systems are predominately ruled by nearest neighbor interactions which show that from this point of view, the quasi-chemical approach applied in section 5.4 is appropriate. From Boltzmann statistics it is in principle possible to calculate the inter-particle interaction energy from the relation

$$g(j) = \exp(-V_{eff}(j)/kT) \quad (5.10)$$

The interaction energy  $V_{eff}(j)$  is the so called potential of mean force which describes the interaction of a particle within an ensemble of other particles. Only in the limit of  $\Theta \rightarrow 0$  this quantity equals the pair potential  $E_{int}$  which is used in equation 5.5. At higher  $\Theta$ , contributions e.g. from entropic forces have to be taken into account [108]. Therefore, the potential of mean force has been calculated only for low fullerene coverages where a comparison with the pair potential is roughly acceptable. It follows from equation 5.10 that  $V_{eff}(1) = +10 \pm 3$  meV for  $C_{60}$  (at  $\Theta = 0.1$ ) and  $V_{eff}(1) = -10 \pm 3$  meV for  $C_{70}$  (at  $\Theta = 0.2$ ). These values are comparable to the pair interaction energies obtained from the quasi-chemical approach (figure 6c) although they are lower by at least a factor of 2-3. In particular, the opposite sign of the inter-fullerene interaction (attractive for  $C_{70}$  and repulsive for  $C_{60}$  at low coverage) predicted by the quasi-chemical approach is nicely reflected in the pair distribution functions. The change of



sign for the interaction energy of  $C_{60}$  at higher coverage ( $\Theta \geq 0.45$ ) reflects the formation of large fullerene islands which are typically observed under such conditions as exemplarily shown in figure 4.9a. On the other hand, however, it should be noted that both the evaluation of the pair distribution functions and the lattice gas analysis feature as an inherent disadvantage that many-body interactions are completely ignored [109]. Therefore, the presented inter-guest interaction energies should be regarded as a first order approximation.

## 5.6 Long-Range Interactions

From a mechanistic point of view, the observed long range interguest interactions can only be mediated through either i) the underlying silver substrate or ii) the porphyrin network. Direct through-space interactions can be ruled out because of the large fullerene-fullerene distance ( $\approx 3.3$  nm) which excludes any significant vdW contributions [110]. Long-range interactions which are mediated via electronic adsorbate-substrate coupling (case i) have been observed for other molecular and atomic systems on surfaces as discussed earlier (section 4.4, surface states). The expected wavelength mentioned there is approximately 3.2 nm and very close to the experimentally observed lateral pore-pore distance of 3.3 nm in the present porphyrin network. Furthermore, the small vertical distances of only a few Angstroms of the fullerenes to the metal substrate likely result in substrate-molecule charge transfer which was reported on purely metallic substrates [111]. A contribution of the Ag substrate to the observed long range inter-fullerene interaction is therefore possible although no experimental evidence is available. This is due to the highly packed porphyrin layer which completely decorates the Ag(111) surface preventing from the observation of standing wave oscillations in such a system. Interactions mediated by the porous organic layer (case ii) can also be expected. This type of inter-guest coupling is attributed to the conformational and electronic modification (e.g. charge transfer processes) of the porphyrin molecules upon adsorption of a fullerene guest. Local distortions in the porphyrin layer induced by a guest molecule are thus assumed to propagate through the porphyrin network, modifying the affinity of neighboring lattice sites to other adsorbates. In the case of the adsorption of  $C_{70}$  within the present porous porphyrin network, the above described mechanisms result in a decrease of the adsorption potential at the nearest neighbor lattice sites around an initially filled pore and thus in the stabilization of individual ad- $C_{70}$ . This kind of interaction can also be supported by the observations made on pure porous DMP layers. As shown in figure 5.8 (and also in figure 5.3) spontaneous changes in the conformation of the porphyrin layer indicated by changes in the brightness of various 3,5di(tert-butyl)phenyl legs can be observed.

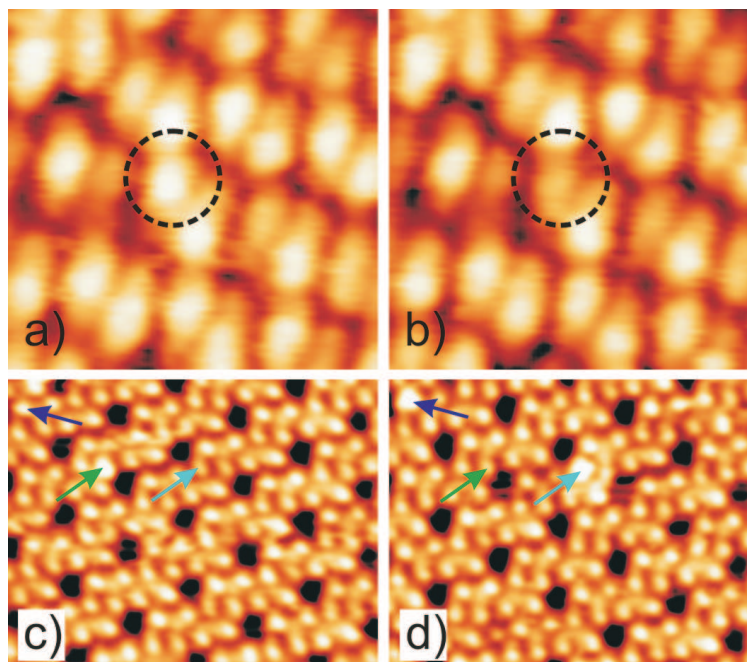


Figure 5.8: Time evolution of the conformations adopted by the 3,5-di(tert-butyl)phenyl substituents in a full monolayer of DDP a), b) (scan range:  $7.8 \times 7.6 \text{ nm}^2$ ,  $V_{bias} = 2.59 \text{ V}$ ,  $I_t = 11 \text{ pA}$ ,  $T = 298 \text{ K}$ , the time lapse between a and b is 92 s) and DMP in the porous phase c), d) (scan range:  $17.5 \times 13.6 \text{ nm}^2$ ,  $V_{bias} = 2.86 \text{ V}$ ,  $I_t = 17 \text{ pA}$ ,  $T = 298 \text{ K}$ , the time lapse between c and d is 62 s). The changes in apparent heights (circle and arrows) reflect the rotation of the 3,5-di(tert-butyl)phenyl substituents around the connecting  $\sigma$ -bond to the porphyrin core.

According to the analysis within the quasi-chemical approach, each additional occupied neighboring pore reduces the interaction potential by a constant value. Overall, this results in a constant and negative pair interaction energy  $E_{int}$  over the whole coverage range, as shown in figure 5.6. Consequently, the hopping rate of the  $C_{70}$  guest molecules decreases rapidly with increasing fullerene coverage, as it is expected for an ideal rigid host lattice [103, 104]. On the other hand, the situation is much more complicated for  $C_{60}$  guest molecules since the interaction energy is dependent on the coverage, changing its sign from positive to negative with increasing coverage. These findings indicate that the  $C_{60}$  guests strongly interact with the porphyrin host and that this interaction is modified with increasing coverage. Such guest-induced modifications of porous networks are well-known from 2D and 3D porous networks, which can even be structurally transformed upon introduction or removal of guest molecules [112–118]. Thereby, physicochemical properties are significantly altered. Due to the high flexibility of the porphyrin molecules in the present network, a similar mechanism is likely to be effective. This idea is further supported by the observation of bright-dim fluctuations of single porphyrin molecules which are propagating through the porous

network, indicating conformational motion of the 3,5-di(tert-butyl)phenyl moieties. Furthermore, the collapse of the porous porphyrin structure upon evaporation of additional guest molecules above the threshold of  $\Theta = 0.8$  is a clear sign of pronounced guest-induced host modifications. From the experiments, however, it is not currently possible to identify the microscopic mechanisms behind the long-range interactions of both  $C_{60}$  and  $C_{70}$ . Most likely, a combination of the two proposed mechanisms is responsible for the observed behavior with different contributions depending on the physical and chemical nature of the guest molecule.



# Chapter 6

## Conclusion and Outlook

Both types of porphyrin molecules, single- and double-core porphyrins, investigated in this work showed pronounced disposition to form ordered layers on metal surfaces. The adsorption of triply-fused di-porphyrins was examined for the first time and resulted in the formation of close-packed monolayers. Large areas of the substrate have been covered with very regular arrangements of these molecules. Furthermore, single-core porphyrins similar to previously studied molecules but featuring different functional side-groups have been deposited. These also proved to self-assemble into various patterns. In addition to close-packed assemblies, these molecules also formed an unprecedented nanoporous layer. Comparison of the various self-assemblies showed that both the functional side-groups and the underlying metal substrate play a crucial role in determining the formation of the monolayers. In general, the porphyrin derivatives examined here proved to be very successful building blocks for self-assembled monolayers on various metal surfaces.

The suitability of these porphyrin structures for hosting fullerene guest molecules has been tested. The porphyrin assemblies have proven to be very effective in order to pattern surfaces for hosting fullerenes. In particular, the nanoporous DMP assembly on Ag(111) can host both C<sub>60</sub> and C<sub>70</sub> fullerenes. Other successful examples were the paired-C<sub>60</sub> phase on DMP/Ag(111) and C<sub>60</sub> on DDP/Ag(100) where the fullerenes prefer to build lines. Interestingly, in all the examined cases the fullerenes adsorbed on top of the cyanophenyl side-group rather than on top of the porphyrin cores. Furthermore, manipulation experiments showed that the adsorbed fullerenes can be addressed and moved individually. The experiments using reversed deposition order (i.e. first C<sub>60</sub> and then porphyrins) have indicated that porphyrin adsorption on top of fullerene monolayers is not very favorable.

A detailed analysis of C<sub>60</sub> and C<sub>70</sub> guest molecules hosted in the nanoporous DMP network has revealed essential differences between the respective interactions. Firstly, the hopping rates at low coverage differ by orders of magnitude,

leading to an estimated difference in the jump barrier of  $\approx 0.13$  eV. Furthermore, analysis of the coverage dependent hopping rate has shown that  $C_{60}$  features a coverage dependent guest-guest interaction energy, while the interaction between the  $C_{70}$  stays the same at increased coverage.

The work presented here has clearly shown that self-assembled porphyrin monolayers provide suitable patterned surfaces for hosting fullerenes. Fabrication of self-assembled fullerene structures which are individually addressable might lead to future technologies such as ultra-dense data storage. The host network which responds selectively to different guest molecules opens up the possibility of useability in further nanotechnological applications. Specifically, such properties are interesting for catalysis, gas sorption and surface supported chemistry.

This establishes the possibility for further interesting research. In fact, investigations of the adsorption properties of porphyrins with slightly varied functional groups are ongoing in the *Nanolab*. So far, another porous network has been found, featuring different pore-pore distances and pore diameters. As opposed to varying the functional (cyanophenyl) side-groups, one could also imagine to substitute the other side-groups (3,5-di(tert-butyl)phenyl) by smaller or larger substituents. One would expect to decrease the interaction of the porphyrin core with the metal substrate with increasing size of the legs (and thus increasing the distance between porphyrin and substrate). In order to determine the activation energy more accurately temperature dependent measurements would be an option. By plotting these data into so-called Arrhenius plots one can determine the activation energy  $E_a$  and the attempt frequency  $\nu_0$  of the mobile fullerenes precisely.

# Bibliography

- [1] M. Schulz, *The end of the road for silicon?*, Nature **399**, 729–730 (1999).
- [2] ITRS, *The international technology roadmap for semiconductors: 2005*, Available at <http://public.itrs.net> (2005).
- [3] G. M. Whitesides and B. Grzybowski, *Self-assembly at all scales*, Science **295**, 2418–2421 (2002).
- [4] F. Rosei, *Nanostructured surfaces: challenges and frontiers in nanotechnology*, J. Phys.: Condens. Matter **16**, 1373–1436 (2004).
- [5] M. E. Davis, *Ordered porous materials for emerging applications*, Nature **417**, 813–821 (2002).
- [6] G. D. Fallon, M. A.-P. Lee, S. J. Langford, and P. J. Nichols, *Metalloporphyrin molecular sieves based on tin(IV)porphyrin phenolates*, Org. Lett. **4**, 1895–1898 (2002).
- [7] K. S. Suslick, P. Bhyrappa, J.-H. Chou, M. E. Kosal, S. Nakagaki, D. W. Smithhenry, and S. R. Wilson, *Microporous porphyrin solids*, Acc. Chem. Res. **38**, 283–291 (2005).
- [8] K. Uemura, S. Kitagawa, M. Kondo, K. Fukui, R. Kitaura, H. C. Chang, and T. Mizutani, *Novel flexible frameworks of porous cobalt(III) coordination polymers that show selective guest adsorption based on the switching of hydrogen-bond pairs of amide groups*, Chem. Eur. J. **8**, 3586–3600 (2002).
- [9] F. Schüth and W. Schmidt, *Microporous and mesoporous materials*, Adv. Mater. **14**, 629–637 (2002).
- [10] J.-M. Lehn, *Supramolecular chemistry*, VCH (1995).
- [11] J.-M. Lehn, *Toward self-organization and complex matter*, Science **295**, 2400–2403 (2002).
- [12] G. M. Whitesides, J. P. Mathias, and C. T. Seto, *Molecular self-assembly and nanochemistry: a chemical strategy for the synthesis of nanostructures*, Science **254**, 1312–1319 (1991).

- [13] L. R. Milgrom, *The colours of life: an introduction to the chemistry of porphyrins and related compounds*, Oxford University Press (1997).
- [14] M. B. Crute, *The crystal structure of nickel etioporphyrin-II*, *Acta Cryst.* **12**, 24–28 (1959).
- [15] D. Bonifazi, *From solution to surfaces: synthesis, physical properties, and materials applications of novel fullerene and porphyrin derivatives*, Ph.D. thesis, ETH Zürich (2004).
- [16] H. W. Kroto, J. R. Heath, S. C. O’Brienn, R. F. Curl, and R. E. Smalley, *C<sub>60</sub>: Buckminsterfullerene*, *Nature* **318**, 162–163 (1985).
- [17] K.M. Kadish and R. S. Ruoff, *Fullerenes: chemistry, physics, and technology*, JohnWiley & Sons, Inc. (2000).
- [18] *Official Web Site of the Nobel Foundation, Nobel Prize in Chemistry 1996*, [http://nobelprize.org/nobel\\_prizes/chemistry/laureates/1996/](http://nobelprize.org/nobel_prizes/chemistry/laureates/1996/) (Accessed: 24.08.2006).
- [19] W. Krätschmer, L. D. Lamb, K. Fostiropoulos, and D. R. Huffman, *Solid C<sub>60</sub>: a new form of carbon*, *Nature* **347**, 354–358 (1990).
- [20] T. Sakurai, X. D. Wang, Q. K. Xue, Y. Hasegawa, T. Hashizume, and H. Shinohara, *Scanning tunneling microscopy study of fullerenes*, *Prog. Surf. Sci.* **51**, 263–408 (1996).
- [21] H. B. Bürgi, P. Venugopalan, D. Schwarzenbach, F. Diederich, and C. Thilgen, *The Crystal-Structure of C<sub>70</sub> at 100 K*, *Helv. Chim. Acta* **76**, 2155 (1993).
- [22] M. J. Hardie, P. D. Godfrey, and C. L. Raston, *Self-assembly of grid and helical hydrogen-bonded arrays incorporating bowl-shaped receptor sites that bind globular molecules*, *Chem. Eur. J.* **5**, 1828 (1999).
- [23] C. J. Chen, *Introduction to scanning tunneling microscopy*, Oxford University Press (1993).
- [24] A. Goldoni, C. Cepek, E. Magnano, A. D. Laine, S. Vandre, and M. San-crotti, *Temperature dependence of the electronic structure near  $E_F$  and electron-phonon interaction in C<sub>60</sub>/Ag(100) single layers*, *Phys. Rev. B* **58**, 2228–2232 (1998).
- [25] C. T. Tzeng, W. S. Lo, J. Y. Yuh, R. Y. Chu, and K. D. Tsuei, *Photoemission, near-edge x-ray-absorption spectroscopy, and low-energy electron-diffraction study of C<sub>60</sub> on Au(111) surfaces*, *Phys. Rev. B* **61**, 2263–2272 (2000).



- 
- [26] E. I. Altman and R. J. Colton, *Determination of the orientation of  $C_{60}$  adsorbed on Au(111) and Ag(111)*, Phys. Rev. B **48**, 18244–18249 (1993).
- [27] A. Fartash, *Orientational epitaxy of high-quality  $C_{60}$  films on Ag(111)*, Phys. Rev. B **52**, 7883–7886 (1995).
- [28] W. W. Pai, C. L. Hsu, C. R. Chiang, Y. Chang, and K. C. Lin, *Origin of peculiar STM molecular contrast in  $C_{60}/Ag(100)$* , Surf. Sci. **519**, L605–L610 (2002).
- [29] W. W. Pai, C. L. Hsu, K. C. Lin, L. Y. Sin, and T. B. Tang, *Characterization and control of molecular ordering on adsorbate-induced reconstructed surfaces*, Appl. Surf. Sci. **241**, 194–198 (2005).
- [30] E. Giudice, E. Magnano, S. Rusponi, C. Boragno, and U. Valbusa, *Morphology of  $C_{60}$  thin films grown on Ag(001)*, Surf. Sci. **405**, L561–L565 (1998).
- [31] X. D. Wang, V. Y. Yurov, T. Hashizume, H. Shinohara, and T. Sakurai, *Imaging of  $C_{70}$  Intramolecular Structures with Scanning-Tunneling-Microscopy*, Phys. Rev. B **49**, 14746–14749 (1994).
- [32] J. K. Gimzewski, S. Modesti, T. David, and R. R. Schlittler, *Scanning-tunneling-microscopy of ordered  $C_{60}$  and  $C_{70}$  layers on Au(111), Cu(111), Ag(110), and Au(110) surfaces*, J. Vac. Sci. Technol. B **12**, 1942–1946 (1994).
- [33] Scientific Committee On Emerging and Newly Identified Health Risks (SCENIHR), *modified Opinion (after public consultation) on: The appropriateness of existing methodologies to assess the potential risks associated with engineered and adventitious products of nanotechnologies*, Available at: [http://ec.europa.eu/health/ph\\_risk/committees/04\\_scenihhr/docs/scenihhr\\_o\\_003b.pdf](http://ec.europa.eu/health/ph_risk/committees/04_scenihhr/docs/scenihhr_o_003b.pdf) (Published: March 2006, Accessed: 28.11.2006).
- [34] Michael Crichton, *Prey*, HarperCollins (2002).
- [35] C. Phoenix and E. Drexler, *Safe exponential manufacturing*, Nanotechnology **15**, 869–872 (2004).
- [36] X. C. Zhao, A. Striolo, and P. T. Cummings,  *$C_{60}$  binds to and deforms nucleotides*, Biophys. J. **89**, 3856–3862 (2005).
- [37] E. Oberdörster, *Manufactured nanomaterials (Fullerenes,  $C_{60}$ ) induce oxidative stress in the brain of juvenile largemouth bass*, Environ. Health Perspect. **112**, 1058–1062 (2004).

- [38] G. Brumfiel, *Nanotechnology: A little knowledge ...*, Nature **424**, 246–248 (2003).
- [39] S. Berner, *Molecular diffusion and self-organisation on metal surfaces: sub-phthalocyanine on Ag(111)*, Phd, Universität Basel (2002).
- [40] L. Ramoino, *Adsorption and self-organisation of CuOEP on heterogenous surfaces: tuning the molecule-substrate interaction*, Ph.D. thesis, Universität Basel (2005).
- [41] M. de Wild, *Novel principle for 2D molecular self-assembly: self-intermixed monolayer phases of sub-phthalocyanine and C<sub>60</sub> on Ag(111)*, Ph.D. thesis, Universität Basel (2002).
- [42] G. Binnig and H. Rohrer, *Scanning tunneling microscopy*, Helvetica Physica Acta **55**, 726–735 (1982).
- [43] *Official Web Site of the Nobel Foundation, Nobel Prize in Physics 1986*, [http://nobelprize.org/nobel\\_prizes/physics/laureates/1986/index.html](http://nobelprize.org/nobel_prizes/physics/laureates/1986/index.html) (Accessed: 24.08.2006).
- [44] G. Binnig, H. Rohrer, C. Gerber, and E. Weibel, *7 × 7 reconstruction on Si(111) resolved in real space*, Phys. Rev. Lett. **50**, 120–123 (1983).
- [45] R. Wiesendanger and H.-J. Güntherodt, *Scanning tunneling microscopy III*, Springer-Verlag (1993).
- [46] J. Tersoff and D. R. Hamann, *Theory and application for the scanning tunneling microscope*, Phys. Rev. Lett. **50**, 1998–2001 (1983).
- [47] J. Bardeen, *Tunneling from a many-particle point of view*, Phys. Rev. Lett. **6**, 57 (1961).
- [48] D. Drakova, *Theoretical modelling of scanning tunnelling microscopy, scanning tunnelling spectroscopy and atomic force microscopy*, Rep. Prog. Phys. **64**, 205–290 (2001).
- [49] A. D. Gottlieb and L. Wesoloski, *Bardeen's tunnelling theory as applied to scanning tunnelling microscopy: a technical guide to the traditional interpretation*, Nanotechnology **17**, R57–R65 (2006).
- [50] C. J. Chen, *Theory of scanning tunneling spectroscopy*, J. Vac. Sci. Technol. A **6**, 319–322 (1988).
- [51] P. Sautet, *Images of adsorbates with the scanning tunneling microscope: Theoretical approaches to the contrast mechanism*, Chem. Rev. **97**, 1097–1116 (1997).

- 
- [52] S. Zophel, J. Repp, G. Meyer, and K. H. Rieder, *Determination of binding sites in ordered phases of CO/Cu(211) employing molecular level manipulation*, Chem. Phys. Lett. **310**, 145–149 (1999).
- [53] G. Hörmandinger and J. B. Pendry, *Theoretical calculations of STM data on Ni(100)-C for various concentrations of carbon*, Surf. Sci. **303**, 197–205 (1994).
- [54] T. A. Jung, R. R. Schlitter, J. K. Gimzewski, H. Tang, and C. Joachim, *Controlled room-temperature positioning of individual molecules: Molecular flexure and motion*, Science **271**, 181–184 (1996).
- [55] D. M. Eigler and E. K. Schweizer, *Positioning single atoms with a scanning tunneling microscope*, Nature **344**, 524–526 (1990).
- [56] P. Zeppenfeld, C. P. Lutz, and D. M. Eigler, *Manipulating atoms and molecules with a scanning tunneling microscope*, Ultramicroscopy **42**, 128–133 (1992).
- [57] L. Bartels, G. Meyer, and K. H. Rieder, *Controlled vertical manipulation of single CO molecules with the scanning tunneling microscope: A route to chemical contrast*, Appl. Phys. Lett. **71**, 213–215 (1997).
- [58] L. Bartels, G. Meyer, K. H. Rieder, D. Velic, E. Knoesel, A. Hotzel, M. Wolf, and G. Ertl, *Dynamics of electron-induced manipulation of individual CO molecules on Cu(III)*, Phys. Rev. Lett. **80**, 2004–2007 (1998).
- [59] G. Meyer, B. Neu, and K. H. Rieder, *Controlled lateral manipulation of single molecules with the scanning tunneling microscope*, Appl. Phys. A-Mater. Sci. Process. **60**, 343–345 (1995).
- [60] J. K. Gimzewski and C. Joachim, *Nanoscale science of single molecules using local probes*, Science **283**, 1683–1688 (1999).
- [61] P. H. Beton, A. W. Dunn, and P. Moriarty, *Room temperature manipulation of C<sub>60</sub> molecules on a Si surface*, Surf. Sci. **362**, 878–881 (1996).
- [62] P. H. Beton, A. W. Dunn, and P. Moriarty, *Manipulation of C<sub>60</sub> molecules on a Si surface*, Appl. Phys. Lett. **67**, 1075–1077 (1995).
- [63] H. Tang, M. T. Cuberes, C. Joachim, and J. K. Gimzewski, *Fundamental considerations in the manipulation of a single C<sub>60</sub> molecule on a surface with an STM*, Surf. Sci. **386**, 115–123 (1997).
- [64] M. T. Cuberes, R. R. Schlittler, and J. K. Gimzewski, *Manipulation of C<sub>60</sub> molecules on Cu(111) surfaces using a scanning tunneling microscope*, Appl. Phys. A-Mater. Sci. Process. **66**, S669–S673 (1998).

- [65] A. W. Dunn, P. H. Beton, and P. Moriarty, *C<sub>60</sub> manipulation and cluster formation using a scanning tunneling microscope*, J. Vac. Sci. Technol. B **14**, 1596–1599 (1996).
- [66] J. K. Gimzewski, T. A. Jung, M. T. Cuberes, and R. R. Schlittler, *Scanning tunneling microscopy of individual molecules: beyond imaging*, Surf. Sci. **386**, 101–114 (1997).
- [67] T. A. Jung, R. R. Schlitter, and J. K. Gimzewski, *Conformational identification of individual adsorbed molecules with the STM*, Nature **386**, 696–698 (1997).
- [68] F. Moresco, G. Meyer, K.-H. Rieder, H. Tang, A. Gourdon, and C. Joachim, *Conformational changes of single molecules induced by scanning tunneling microscopy manipulation: A route to molecular switching*, Phys. Rev. Lett. **86**, 672–675 (2001).
- [69] T. Yokoyama, S. Yokoyama, T. Kamikado, Y. Okuno, and S. Mashiko, *Selective assembly on a surface of supramolecular aggregates with controlled size and shape*, Nature **413**, 619–621 (2001).
- [70] Y. Kang, S. S. Lee, K.-M. Park, S. H. Lee, S. O. Kang, and J. Ko, *Self-assembly of one-dimensional coordination polymers from AgX (X = CF<sub>3</sub>SO<sub>3</sub><sup>-</sup>, ClO<sub>4</sub><sup>-</sup>, and NO<sub>3</sub><sup>-</sup>) and 2-aminomethylpyridinedipropionitrile (2-AMPDPN)*, Inorg. Chem. **40**, 7027–7031 (2001).
- [71] S. Berner, M. Brunner, L. Ramoino, H. Suzuki, H.-J. Güntherodt, and T. A. Jung, *Time evolution analysis of a 2D solid-gas equilibrium: a model system for molecular adsorption and diffusion*, Chem. Phys. Lett. **348**, 175–181 (2001).
- [72] S. Berner, M. de Wild, L. Ramoino, S. Ivan, A. Baratoff, H.-J. Güntherodt, H. Suzuki, D. Schlettwein, and T. A. Jung, *Adsorption and two-dimensional phases of a large polar molecule: Sub-phthalocyanine on Ag(111)*, Phys. Rev. B **68**, 115410 (2003).
- [73] J. Kuntze, X. Ge, and R. Berndt, *Chiral structures of lander molecules on Cu(100)*, Nanotechnology **15**, 337–340 (2004).
- [74] T. Steiner, *The hydrogen bond in the solid state*, Angew. Chem.-Int. Edit. **41**, 48–76 (2002).
- [75] M. de Wild, S. Berner, H. Suzuki, H. Yanagi, D. Schlettwein, S. Ivan, A. Baratoff, H.-J. Güntherodt, and T. A. Jung, *A novel route to molecular self-assembly: Self-intermixed monolayer phases*, Chem. Phys. Chem. **10**, 881 (2002).

- [76] C. Pan, M. P. Sampson, Y. Chai, R. H. Hauge, and J. L. Margrave, *Heats of sublimation from a polycrystalline mixture of C<sub>60</sub> and C<sub>70</sub>*, J. Phys. Chem. **95**, 2944–2946 (1991).
- [77] D. Bonifazi, M. Scholl, F. Y. Song, L. Echegoyen, G. Accorsi, N. Armaroli, and F. Diederich, *Exceptional redox and photophysical properties of a triply fused diporphyrin-C<sub>60</sub> conjugate: Novel scaffolds for multicharge storage in molecular scale electronics*, Angew. Chem.-Int. Edit. **42**, 4966–4970 (2003).
- [78] M. Böhringer, W. D. Schneider, and R. Berndt, *Scanning tunneling microscope-induced molecular motion and its effect on the image formation*, Surf. Sci. **408**, 72–85 (1998).
- [79] N. W. Ashcroft and N. D. Mermin, *Solid state physics*, Harcourt College Publishers (1976).
- [80] A. Zangwill, *Physics at surfaces*, Cambridge University Press (1988).
- [81] D. H. Everett, *Manual of symbol and terminology for physicochemical quantities and units, appendix: definitions, terminology and symbols in colloid and surface chemistry*, Pure Appl. Chem. **31**, 579–638 (1972), available online at: <http://www.iupac.org/reports/1972/3104everett/>.
- [82] J. W. Steed, *Supramolecular chemistry*, Wiley (2000).
- [83] L. Scudiero, D. E. Barlow, and K. W. Hipps, *Scanning tunneling microscopy, orbital-mediated tunneling spectroscopy, and ultraviolet photoelectron spectroscopy of nickel(II) octaethylporphyrin deposited from vapor*, J. Phys. Chem. B **106**, 996–1003 (2002).
- [84] P. A. Stevens, R. J. Madix, and J. Stöhr, *The bonding of acetonitrile and CH<sub>2</sub>CN on Ag(110) determined by near edge x-ray absorption fine-structure: Evidence for π-donor bonding and azimuthal ordering*, J. Chem. Phys. **91**, 4338–4345 (1989).
- [85] V. S. Stepanyuk, A. N. Baranov, D. V. Tsivlin, W. Hergert, P. Bruno, N. Knorr, M. A. Schneider, and K. Kern, *Quantum interference and long-range adsorbate-adsorbate interactions*, Phys. Rev. B **68**, 205410 (2003).
- [86] M. F. Crommie, C. P. Lutz, and D. M. Eigler, *Confinement of electrons to quantum corrals on a metal-surface*, Science **262**, 218–220 (1993).
- [87] N. Knorr, H. Brune, M. Epple, A. Hirstein, M. A. Schneider, and K. Kern, *Long-range adsorbate interactions mediated by a two-dimensional electron gas*, Phys. Rev. B **65**, 115420 (2002).

- [88] S. Lukas, G. Witte, and Ch. Wöll, *Novel mechanism for molecular self-assembly on metal substrates: Unidirectional rows of pentacene on Cu(110) produced by a substrate-mediated repulsion*, Phys. Rev. Lett. **88**, 028301 (2002).
- [89] F. Silly, M. Pivetta, M. Ternes, F. Patthey, J. P. Pelz, and W.-D. Schneider, *Creation of an atomic superlattice by immersing metallic adatoms in a two-dimensional electron sea*, Phys. Rev. Lett. **92**, 016101 (2004).
- [90] E. C. H. Sykes, B. A. Mantooh, P. Han, Z. J. Donhauser, and P. S. Weiss, *Substrate-mediated intermolecular interactions: A quantitative single molecule analysis*, J. Am. Chem. Soc. **127**, 7255–7260 (2005).
- [91] M. Ternes, C. Weber, M. Pivetta, F. Patthey, J. P. Pelz, T. Giamarchi, F. Mila, and W.-D. Schneider, *Scanning-tunneling spectroscopy of surface-state electrons scattered by a slightly disordered two-dimensional dilute "solid": Ce on Ag(111)*, Phys. Rev. Lett. **93**, 146805 (2004).
- [92] J. Repp, F. Moresco, G. Meyer, K.-H. Rieder, P. Hyldgaard, and M. Persson, *Substrate mediated long-range oscillatory interaction between adatoms: Cu/Cu(111)*, Phys. Rev. Lett. **85**, 2981–2984 (2000).
- [93] S. Stepanow, M. Lingenfelder, A. Dmitriev, H. Spillmann, E. Delvigne, N. Lin, X. B. Deng, C. Z. Cai, J. V. Barth, and K. Kern, *Steering molecular organization and host-guest interactions using two-dimensional nanoporous coordination systems*, Nat. Mater. **3**, 229–233 (2004).
- [94] N. Katsonis, A. Marchenko, and D. Fichou, *Adsorption and self-assembly of C<sub>70</sub> molecules at the Au(111)/n-tetradecane interface: A scanning tunneling microscopy study*, Adv. Mater. **16**, 309 (2004).
- [95] D. M. Cyr, B. Venkataraman, G. W. Flynn, A. Black, and G. M. Whitesides, *Functional group identification in scanning tunneling microscopy of molecular adsorbates*, J. Phys. Chem. **100**, 13747–13759 (1996).
- [96] H. Fukumura, D. L-i, H. Uji-i, S. Nishio, H. Sakai, and A. Ohuchi, *Image contrast analysis of STM images of self-assembled dioctadecyl chalcogenides on graphite at the liquid-solid interface*, ChemPhysChem **6**, 2383–2388 (2005).
- [97] H. B. Bürgi, E. Blanc, D. Schwarzenbach, S. Liu, Y. Lu, M. M. Kappes, and J. A. Ibers, *The structure of C<sub>60</sub> - orientational disorder in the low-temperature modification of C<sub>60</sub>*, Angew. Chem. Int. Ed. **31**, 640 (1992).
- [98] K. Hedberg, L. Hedberg, D. S. Bethune, C. A. Brown, H. C. Dorn, R. D. Johnson, and M. De Vries, *Bond lengths in free molecules of buckminsterfullerene, C<sub>60</sub>, from gas-phase electron-diffraction*, Science **254**, 410 (1991).



- 
- [99] B. G. Briner, M. Doering, H. P. Rust, and A. M. Bradshaw, *Microscopic molecular diffusion enhanced by adsorbate interactions*, *Science* **278**, 257–260 (1997).
- [100] J. V. Barth, *Transport of adsorbates at metal surfaces: From thermal migration to hot precursors*, *Surf. Sci. Rep.* **40**, 75–149 (2000).
- [101] B. G. Briner, M. Doering, H. P. Rust, and A. M. Bradshaw, *Mobility and trapping of molecules during oxygen adsorption on Cu(110)*, *Phys. Rev. Lett.* **78**, 1516–1519 (1997).
- [102] M. Schunack, T. R. Linderoth, F. Rosei, E. Laegsgaard, I. Stensgaard, and F. Besenbacher, *Long jumps in the surface diffusion of large molecules*, *Phys. Rev. Lett.* **88**, 156102 (2002).
- [103] D. A. Reed and Ehrlich. G., *Surface-diffusion, atomic jump rates and thermodynamics*, *Surf. Sci.* **102**, 588–609 (1981).
- [104] R. Krishna, D. Paschek, and R. Baur, *Modeling the occupancy dependence of diffusivities in zeolites*, *Microporous Mesoporous Mater.* **76**, 233–246 (2004).
- [105] D. A. Reed and Ehrlich. G., *Surface diffusivity and the time correlation of concentration fluctuations*, *Surf. Sci.* **105**, 603–628 (1981).
- [106] R. Gomer, *Diffusion of adsorbates on metal-surfaces*, *Rep. Prog. Phys.* **53**, 917–1002 (1990).
- [107] D. L. Meixner and S. M. George, *Surface diffusion of xenon on Pt(111)*, *J. Chem. Phys.* **98**, 9115 (1993).
- [108] J. Trost, T. Zambelli, J. Wintterlin, and G. Ertl, *Adsorbate-adsorbate interactions from statistical analysis of STM images: N/Ru(0001)*, *Phys. Rev. B* **54**, 17850–17857 (1996).
- [109] L. Österlund, M. O. Pedersen, I. Stensgaard, E. Laesgaard, and F. Besenbacher, *Quantitative determination of adsorbate-adsorbate interactions*, *Phys. Rev. Lett.* **83**, 4812–4815 (1999).
- [110] L. A. Girifalco, M. Hodak, and R. S. Lee, *Carbon nanotubes, buckyballs, ropes and a universal graphitic potential*, *Phys. Rev. B* **62**, 13104 (2000).
- [111] L.-L. Wang and H.-P. Cheng, *Density functional study of the adsorption of a C<sub>60</sub> monolayer on Ag(111) and Au(111) surfaces*, *Phys. Rev. B* **69**, 165417 (2004).

- [112] S. Aitipamula and A. Nangia, *Guest-induced supramolecular isomerism in inclusion complexes of T-shaped host 4,4-bis(4'-hydroxyphenyl) cyclohexanone*, Chem. Eur. J. **11**, 6727 (2005).
- [113] L. Dobrzanska, G. O. Lloyd, H. G. Raubenheimer, and L. J. Barbour, *A discrete metallocyclic complex that retains its solvent-templated channel structure on guest removal to yield a porous, gas sorbing material*, J. Am. Chem. Soc. **127**, 13134–13135 (2005).
- [114] S. Kitagawa, R. Kitaura, and S. Noro, *Functional porous coordination polymers*, Angew. Chem.-Int. Edit. **43**, 2334–2375 (2004).
- [115] C. Mellot-Draznieks, C. Serre, S. Surblé, N. Audebrand, and G. Férey, *Very large swelling in hybrid frameworks: A combined computational and powder diffraction study*, J. Am. Chem. Soc. **127**, 16273 (2005).
- [116] K. Uemura, S. Kitagawa, K. Fukui, and K. Saito, *A contrivance for a dynamic porous framework: Cooperative guest adsorption based on square grids connected by amide-amide hydrogen bonds*, J. Am. Chem. Soc. **126**, 3817–3828 (2004).
- [117] D. X. Wu, K. Deng, Q. D. Zeng, and C. Wang, *Selective effect of guest molecule length and hydrogen bonding on the supramolecular host structure*, J. Phys. Chem. B **109**, 22296–22300 (2005).
- [118] J. P. Zhang, Y. Y. Lin, W. X. Zhang, and X. M. Chen, *Temperature- or guest-induced drastic single-crystal-to-single-crystal transformations of a nanoporous coordination polymer*, J. Am. Chem. Soc. **127**, 14162–14163 (2005).



# Acknowledgements

I would like to thank the following people who all helped in making this PhD project a success:

- Prof. Dr. H.-J. Güntherodt and Dr. T. Jung for giving me the opportunity to work in the *Nanolab*.
- Prof. E. Meyer for agreeing to be a referee for this thesis.
- Dr. H. Spillmann for agreeing to be my supervisor and for all his help in the lab and while writing papers.
- Dr. S. Berner and Dr. M. de Wild for introducing me to the group and for teaching me the secrets of the *Nanolab*.
- All the current and former group members (Dr. M. Stöhr, Dr. L. Ramoino, Dr. M. von Arx, Dr. M. Wahl, N. Wintjes, T. Samuely, M. Matena, S. Boz, A. Heuri, D. Haldeman, S. Schnell) for their continuous help and interesting discussions.
- The group of Prof. F. Diederich (especially Dr. D. Bonifazi, J. Hornung, L.-A. Fendt and M. Schär) for supplying us with great molecules and for invaluable scientific discussions.
- The mechanical and electrical workshops and the secretaries for keeping things running smoothly.
- My friends and family for their support. In particular R. Huber, L. Zimmerli, Dr. T. Gyalog, Dr. M. Guggisberg for having lunch with me and for the great physics outreach projects we had the opportunity to participate in. M. Frischknecht and Ph. Meili for sharing a flat with me and great discussions about chemistry. Ch. Buser for his support with statistical questions.



# Publications and Conferences

## Conference Presentations

- 12.10.2006 **International Symposium: Complex Molecular Architectures on Surfaces**, Bonn, Germany. Poster  
*Adsorption and Coverage Dependent Dynamics of Long-Range Interacting Fullerenes in a Flexible Two-Dimensional Nanoporous Porphyrin Network*
- 31.7.-4.8.2006 **ICN&T**, Basel, Switzerland. Poster  
*Adsorption and Coverage Dependent Dynamics of Long-Range Interacting Fullerenes in a Flexible Two-Dimensional Nanoporous Porphyrin Network*
- 13.3.-17.3.2006 **APS March Meeting 06**, Baltimore, USA. Oral presentation  
*A Two-dimensional Porphyrin-based Porous Network Featuring Communicating Cavities*
- 6.10.-7.10.2005 **Annual NCCR Nano Meeting**, Gwatt, Switzerland. Poster  
*A Two-dimensional Porphyrin-based Porous Network Featuring Communicating Cavities for the Templated Complexation of Fullerenes*
- 20.2.-25.2.2005 **NanoTech Insight'05**, Luxor, Egypt. Oral presentation  
*Supramolecular C<sub>60</sub>/Porphyrin Assemblies on Metals*
- 21.5.2004 **Columbia University**, New York, USA. Colloquium talk  
*Supramolecular C<sub>60</sub>/Porphyrin Assemblies on Metal Surfaces*
- 14.6.-18.6.2004 **fPi6**, Ithaca, NY, USA. Oral presentation  
*Supramolecular [60]Fullerene/Porphyrin Assemblies on Metals*
- 3.3.-4.3.2004 **SPS '04**, Neuchâtel, Switzerland. Oral presentation  
*Fullerene-Porphyrin assemblies on metal surfaces investigated with STM - Towards functional surfaces*

## Publications

- 2006 *Adsorption and Dynamics of Long-Range Interacting Fullerenes in a Flexible, Two-Dimensional, Nanoporous Porphyrin Network*  
ChemPhysChem **7**, 1462-1470 (2006)  
DOI: 10.1002/cphc.200600186
- 2006 *A Two-Dimensional Porphyrin-Based Porous Network Featuring Communicating Cavities for the Templated Complexation of Fullerenes*  
Adv. Mater. **18**, 275-279 (2006)  
DOI: 10.1002/adma.200501734
- 2004 *Supramolecular Patterned Surfaces Driven by Cooperative Assembly of C<sub>60</sub> and Porphyrins on Metal Substrates*  
Angew. Chem. Int. Ed. **43**, 4759-4763(2004)  
DOI: 10.1002/ange.200460562

## Patents

- 2006 N. Wintjes, H. Spillmann, D. Bonifazi, A. Kiebele, F. Cheng, H.-J. Güntherodt, T. Jung and F. Diederich  
*A molecular three way rotary switch also able to store information hosted by a molecular matrix*  
US patent 60/831,111, filed 14. 7. 2006, pending.
- 2005 H. Spillmann, D. Bonifazi, A. Kiebele, F. Cheng, H.-J. Güntherodt, T. Jung, F. Diederich  
*Method for building a two-dimensional nanostructure comprising a regular arrangement of interacting /communicating nanopores by molecular self-organization on surfaces*  
US provisional patent application filed 17. 8. 2005
- 2005 H. Spillmann, D. Bonifazi, A. Kiebele, M. de Wild, P. Seiler, F. Cheng, H.-J. Güntherodt, T. Jung and F. Diederich  
*Method for building bi-molecular nanoscale patterns by cooperative self-organization on surfaces*  
US provisional patent application filed 2. 3. 2005

# Curriculum Vitae

von Andreas Kiebele, geboren am 25.4.1977

## Ausbildung

- seit 11.2003 Doktorand am Institut für Physik, **Universität Basel**
- 09.1998-10.2003 Physik Studium an der **Universität Basel**.  
Abschluss: Diplom in Experimentalphysik.
- 09.1994-06.1995 **Auslandsaufenthalt** in den USA  
Abschluss: High-School Diploma an der Tuscaloosa County High School. 'Awards of Honor for Outstanding Academic Achievement' in Algebra II und American History.
- 08.1993-12.1997 **Gymnasium Münchenstein**, BL, Typus C (Naturwissenschaften).

## Berufserfahrung

- 01.2004-03.2006 **World Year of Physics 2005**  
Konferenz- und Ausstellungsorganisation, Aufbau und Unterhalt Webseite, Koordination von Nationalen und Internationalen Events
- Sommer 2001-2004 **Schwimmbad Aesch-Pfeffingen**, Badeaufsicht
- 12.1997-07.2002 **Metrowerks**, Basel, Aushilfe im Technischen Marketing

Folgenden Dozentinnen und Dozenten verdanke ich meine Ausbildung:

C. Bandle, R. Benewitz, C. Bruder, H. Burkhart, A. Bussmann-Holder, D. Masser, E. Meyer, H.-J. Güntherodt, M. Hegner, G.-R. Plattner, I. Sick, T. A. Jung, C. Schönenberger, L. Tauscher, F.-K. Thielemann, D. Trautmann